Protocatechuic acid induces endogenous oxidative stress in CR-hvKP by regulating the EMP-PPP pathway

Yesheng Zhong1,Yumeng Cheng2,Shuai Xing1,Xiaoxiao Zhang3,Shiqi Luo1,Xinru Shi1,Yang He1,Huixin Liu1,Meng Yang1,Hongbin Si1*

1College of AnimaScience and Technology, Guangxi KeyLaboratory of Animal Breeding, DiseaseControl and Prevention, Nanning, 530004, PRChina
2College of Animal Sciences, Fujian Agriculture and Forestry University, Fuzhou, 350002, China
3College of Life Sciences, Northwest A&F University, Yangling, Shaanxi, 712100, China
*Corresponding Author: Prof: Hongbin Si, shb2009@gxu.edu.cn

ABSTRACT

Background: Klebsiella pneumoniae is an important opportunistic pathogen and zoonotic pathogen. The widespread use of antibiotics has led to the emergence of a large number of multidrug-resistant Klebsiella pneumoniae in clinical animal husbandry, posing a serious threat to global health security. Protocatechuic acid (PCA) is a phenolic acid substance naturally present in many vegetables and fruits. It is a safe and highly developed new type of antibacterial synergist.

Purpose: This study explored the antibacterial and synergistic mechanisms of PCA against Carbapenem-resistant hypervirulent Klebsiella pneumoniae.

Study design: Metabolomic analysis using PCA to investigate the metabolic effects of CR-hvKP and further explore the antibacterial mechanisms resulting from this metabolic regulation.

Methods: The MIC of PCA was measured by microdilution, and its bactericidal effect was observed by DAPI staining. Resistance and hemolysis tests were performed to ensure safety. The synergy of PCA and meropenem was tested by checkerboard assay. The biofilm inhibition was assessed by crystal violet and EPS assays. The membrane morphology, permeability, and potential were examined by SEM, PI, NPN, and DiSC3(5). The metabolic changes were evaluated by AlamarBlue, metabolomics, enzyme activity, ELISA, molecular docking, and qRT-PCR. The oxidative stress and metabolic disorders were verified by NADP(H), ROS, MDA, and ATP assays.

Results: The results showed that PCA can synergize with antibiotics and inhibit the biofilm and membrane functions of CR-hvKP at low concentrations. Metabolomics revealed that PCA affects the EMP and PPP pathways of CR-hvKP, causing oxidative stress. This involves the binding of PGAM and the downregulation of BPGM, leading to the accumulation of glycerate-3P. This results in the inhibition of G6PDH and the imbalance of NADPH/NADP+, disrupting the energy metabolism and increasing the oxidative stress, which impair the biofilm and membrane functions and enhance the antibiotic efficacy.

Conclusion: The results demonstrate that PCA regulates the EMP-linked PPP pathway of CR-hvKP, inhibits biofilm and membrane functions, and synergizes with antibiotics to kill bacteria, providing new insights and candidates for natural antibacterial enhancers.

Author Summary

Klebsiella pneumoniae is a common pathogenic bacterium that can infect both humans and animals, causing serious diseases such as pneumonia, meningitis, and sepsis. Due to the overuse of antibiotics, this bacterium has developed resistance to many drugs, posing a significant threat to global health security. Through our research, we have discovered a natural substance called protocatechuic acid (PCA) that can enhance the effectiveness of antibiotics against this bacterium. PCA is found in many vegetables and fruits and is a safe and non-toxic antibacterial adjuvant. Our analysis of the metabolomics of PCA on Klebsiella pneumoniae has revealed its antibacterial and synergistic mechanisms. The study found that PCA can affect the bacterium's sugar metabolism pathway, leading to the generation of endogenous oxidative stress. This disrupts their energy metabolism, damages their cell membranes and biofilms, making them more susceptible to being killed by antibiotics. Through this mechanism, PCA can synergize with common antibiotics such as meropenem, enhancing their bactericidal ability. Our research has demonstrated that PCA is an effective antibacterial adjuvant, providing new candidates and insights for the development of natural antibacterial agents.

63

64 Graphical abstract

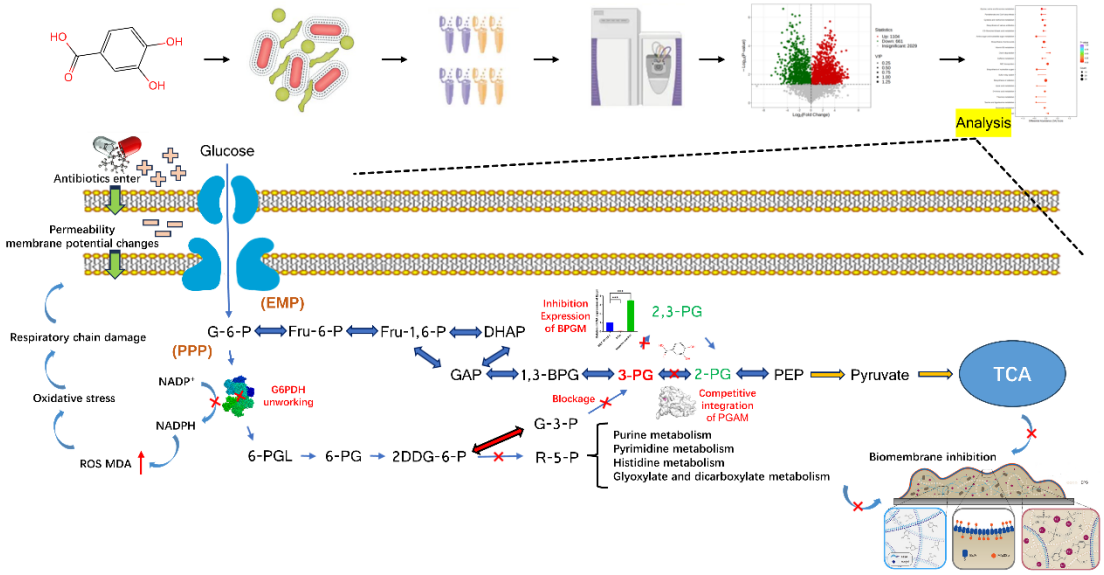

65

66 Keywords: Carbapenem-resistant hypervirulent Klebsiella pneumoniae; Protocatechuic acid;

67 Glycolysis; Pentose phosphate pathway; Oxidative stress

68

1 Introduction

Klebsiella pneumoniae is a Gram-negative bacterium widely distributed in the skin, respiratory and digestive tracts, urinary and reproductive systems of humans and animals, as well as in the natural environment. It is an important opportunistic pathogen and zoonotic pathogen, capable of causing severe infectious diseases such as pneumonia, sepsis, urinary tract infections, and meningitis. It can be transmitted to humans and animals through the food chain or direct contact, posing a threat to public health and animal husbandry[1]. Due to the widespread use and abuse of broad-spectrum antibiotics, Klebsiella pneumoniae has developed multiple drug resistance, especially resistance to carbapenems, making the treatment of Klebsiella pneumoniae infections extremely difficult. In recent years, genetic elements involved in the exchange of carbapenemase-producing cKP and hvKP have been discovered, indicating the emergence of carbapenem-resistant hypervirulent Klebsiella pneumoniae (CR-hvKP). CR-hvKP not only produces carbapenemases, leading to resistance to carbapenems, but also expresses various virulence factors such as collagenase, siderophore, and capsule, enhancing its invasiveness and lethality [3-4]. CR-hvKP has been reported in multiple countries and regions worldwide, becoming a new clinical challenge and public health threat [4].

Therefore, it is urgently needed to search for new antibacterial agents to combat CR-hvKP infection. Natural plant antibacterial agents refer to substances with antibacterial activity extracted or synthesized from plants, such as flavonoids, phenolic acids, tannins, anthocyanins, etc. These

substances have the characteristics of being natural, safe, non-toxic, and free of side effects, and will not cause harm to the human body and animals [5]. Natural plant antibacterial agents have multi-target and multi-mechanism antibacterial properties, which can affect the growth and reproduction of bacteria in different ways, such as destroying cell walls and membranes, changing membrane potential and energy metabolism, and inhibiting the synthesis of biomacromolecules [6]. These methods can effectively combat infections caused by multidrug-resistant bacteria and provide new strategies for the treatment of refractory diseases. Protocatechuic acid (PCA), also known as 3,4-dihydroxybenzoic acid, is a phenolic acid substance naturally present in many vegetables and fruits, such as blackberries, strawberries, cherries, grapes, tea, etc. [7]. PCA has various biological activities such as antioxidant, anti-inflammatory, and anti-tumor effects, which can eliminate free radicals, inhibit the release of inflammatory factors, and induce apoptosis of cancer cells [8]. PCA also has certain antibacterial effects and can inhibit the growth of various bacteria, such as Staphylococcus aureus, Escherichia coli, Salmonella, etc. [9-10]. Moreover, PCA can inhibit the biofilm formation of Klebsiella pneumoniae by inhibiting its quorum sensing [11]. However, the antibacterial effect of PCA on CR-hvKP and its mechanism have not been fully studied.

In this study, we demonstrated that PCA promotes the disruption of intracellular redox balance by affecting key enzymes in the CR-hvKP metabolic process, leading to changes in membrane permeability and inhibition of biofilm function, ultimately synergizing with antibiotics to kill drug-resistant bacteria.

2 Materials and Methods

2.1 Bacteria strains

Klebsiella pneumoniae (MEC19116-1) and Klebsiella pneumoniae (FMEC20113-2), these two strains are carbapenem-resistant Klebsiella pneumoniae (CRKP) selected from samples of edible animals and their surrounding growth environment. After preliminary identification of virulence genes, both strains were found to have highly virulent genes. They were cultured in LB medium at 37°C.

2.2 Chemicals and reagents

Protocatechuic acid is purchased from Hengrui Tongda Company. Congo red, sucrose, glucose, and KCl are products of Glucose Company. Dimethyl sulfoxide, meropenem, tigecycline, dexamethasone, DAPI, PI, HEPES buffer, AlamarBlue, ROS detection kit, NADP(H) detection kit, and G6PDH enzyme detection kit are products of Solarbio Company. ATP detection kit and MDA detection kit are products of Biyun Tian Company. DisC3(5) and NPN are products of Aladdin Company. Glycerate-3P is a product of Shanghai Yuan Ye Biotechnology Co., Ltd. PGAM enzyme-linked immunosorbent assay kit and BPGM enzyme-linked immunosorbent assay kit are products of MEIMIAN Company. Bacteria RNA Extraction Kit, reverse transcription kit, and qRT-PCR detection dye are products of Genstar Company.

2.3 Minimum inhibitory concentration and minimum bactericidal concentration

Add an appropriate concentration of PCA to the liquid culture medium and dilute it into different

concentrations of drug culture medium. Take a certain volume of bacterial suspension and mix it with each concentration of medium in a 96-well plate. Place the prepared 96-well plate in a bacterial incubator for overnight incubation. Based on the growth of bacteria in the 96-well plate, the drug concentration corresponding to the last area without white spots of bacterial growth can determine the minimum inhibitory concentration (MIC) of the drug. To determine the minimum bactericidal concentration (MBC), take 10μL of the culture fluid from the MIC well and the two wells on the left side of the drug concentration, and inoculate them on a drug-free agar plate. After average spreading, incubate again overnight in a 35℃ incubator with normal air. The lowest drug concentration required to kill 99.9% (reducing by 3 orders of magnitude) of the test microorganisms is defined as the MBC [12].

2.4 Time-dependent inhibition curve

Prepare LB medium according to the preparation method and sterilize it. Add different concentrations of PCA and inoculate bacteria in the logarithmic growth phase into the medium. Place the inoculated medium in a constant temperature shaker for cultivation. Use a spectrophotometer to regularly measure the bacterial quantity. Based on the measured bacterial quantity data, plot the bacterial growth curve [13].

2.5 DAPI staining

After culturing bacteria to the logarithmic growth phase, different concentrations of PCA were added and incubated for 30 minutes. The cells were then collected by centrifugation at 4℃ and 5000rpm for 5 minutes. The cells were washed three times with PBS buffer and DAPI was added

158 to precipitate. Subsequently, the cells were treated in the dark for 20 minutes, followed by
159 centrifugation at 5000rpm for 3 minutes and three additional washes with PBS buffer. The cells
160 were resuspended in 100μL of PBS buffer and 10μL was taken onto a glass slide. A cover glass
161 was placed on top and the cells were observed under a fluorescence microscope and photographed
162 [14].
163
164 2.6 Hemolysis assay
165 Take 5mL of mammalian blood using an anticoagulant tube, centrifuge at 1000g for 10 minutes
166 under a frozen centrifuge, pour off the supernatant, slowly add physiological saline and invert
167 repeatedly until well mixed, repeat centrifugation 2-3 times until a clear supernatant is obtained,
168 and dilute it to a 5% red blood cell suspension. Dilute the original chlorogenic acid to different
169 concentrations of drug groups using physiological saline, and set up a physiological saline group
170 and a prednisolone group. Mix the red blood cell suspension with the drug solution and add it to a
171 96-well cell plate, incubate at 37°C on a shaker for 1 hour, centrifuge at 1000g for 10 minutes at
172 4°C, transfer a certain amount of supernatant to another 96-well cell plate, and add an equal
173 volume of physiological saline. Measure the absorbance at 540nm [15].
174
175 2.7 Research on the development of drug resistance
176 The overnight shaken bacteria were inoculated into a new broth culture medium and added with
177 1/2 MIC concentration of PCA and positive control drug tetracycline, and incubated on a shaker
178 for 12 hours as one generation. Then, the bacteria were taken out for drug sensitivity test and
179 continued to be subcultured. The concentration of the drugs added should be maintained at 1/2

MIC. Finally, it was subcultured until the twentieth generation and a drug sensitivity curve was plotted [16].

2.8 Checkerboard experiments

The PCA and meropenem were separately diluted in a 96-well plate, and then they were mixed in equal proportions to form multiple drug combinations with different concentrations. An equal volume of bacterial suspension was added afterwards. Positive and negative control groups need to be designed in the experiment. The prepared 96-well plate was placed in a bacterial incubator for overnight incubation, and the drug concentration corresponding to the area without white spots in the 96-well plate was recorded. The formula for the result is FICI = MICab/MICa + MICba/MICb [17].

2.9 Characterization of metabolism observations

Using 0.08g of Congo red, 5g of sucrose, 1g of agar, 5g of brain-heart infusion medium, 200mL of deionized water, and different concentrations of PCA as Congo red medium, the bacteria were inoculated in liquid medium containing 5% glucose and cultured for 24 hours. Then, 10μL of bacterial suspension was taken and inoculated onto Congo red solid medium, followed by incubation at 37℃ for 24 hours. Afterwards, the plates were taken out and observed at room temperature. If the colonies appeared black, it indicated that the bacteria were biofilm-positive; if the colonies appeared red, it indicated that the bacteria were biofilm-negative [18].

2.10 Crystal violet staining

Bacteria with a logarithmic growth phase were inoculated into a 96-well plate containing LB medium at a concentration of 10^6 CFU/mL, with 200μL per well. The plate was set up with a positive control group (containing only bacteria) and different concentrations of PCA groups. The 96-well plate was incubated in a constant temperature incubator at 37°C for 48 hours to allow the bacteria to form a biofilm at the bottom of the wells. The plate was then removed from the incubator, gently tilted, and the culture medium was discarded by shaking. Any remaining liquid was removed using a sterile pipette. Each well was washed three times with sterile PBS buffer, with 200μL per wash, to remove non-adherent cells and impurities. 200μL of a 1% crystal violet solution was added to each well and stained at room temperature for 15 minutes. The crystal violet staining solution was then poured out, and each well was rinsed with tap water until no color overflowed, to remove excess dye. The 96-well plate was inverted and dried on absorbent paper at room temperature or dried at 37°C. 200μL of a 33% acetic acid solution was added to each well and allowed to act at room temperature for 15 minutes to dissolve the crystal violet. The absorbance of each well was measured using an enzyme-linked immunosorbent assay (ELISA) reader at a wavelength of 570nm [19].

2.11 Extracellular polymer content determination test

Cultivate bacteria to the logarithmic growth phase, dilute 100 times and take 2mL of bacteria into a 6-well plate. Place the cell crawler into the well and introduce varying concentrations of PCA. Culture for 48 hours, then use tweezers to remove the scraper and transfer it to a 50mL Eppendorf tube. Perform ice bath sonication for 30 minutes at 4°C, then centrifuge at 4000rpm for 30 minutes under the same conditions. Transfer the supernatant to a 2mL glass tube, add 1mL of

224 phenol and 5mL of concentrated sulfuric acid, and react in the dark for 30 minutes. Measure the
225 absorbance at 490nm wavelength [20].
226
227 2.12 Scanning Electron Microscope
228 Bacteria collected by centrifugation at 3500rpm for 10 minutes and cultured to logarithmic growth
229 phase were resuspended in 1×PBS (PH7.4) three times to OD600=0.5. Then, different
230 concentrations of PCA were added for experimental grouping as shown in the table below, and
231 each test tube was incubated at 37℃ for 4 hours. After incubation, the bacterial suspension was
232 centrifuged at 4000rpm for 10 minutes, resuspended in 1×PBS (PH7.4) three times, and the
233 supernatant was removed to collect the precipitate. The precipitate was fixed in 2.5%
234 glutaraldehyde solution for 2 hours, then washed with PBS to remove the fixative, and
235 sequentially placed in 40%, 50%, 60%, 70%, 80%, and 90% ethanol for 15 minutes for gradient
236 dehydration. It was then replaced with 100% tert-butanol for 30 minutes, dried, gold-coated, and
237 observed and photographed using a scanning electron microscope [21].
238
239 2.13 Inner membrane permeability
240 After culturing bacteria to the logarithmic growth phase, different concentrations of PCA were
241 added and incubated for 30 minutes. Then, 10μL of PI staining solution was added and incubated
242 for another 30 minutes under dark conditions. The samples were transferred to a 96-well cell plate
243 and the fluorescence intensity was measured using an enzyme labeling instrument (excitation
244 wavelength: 535nm; emission wavelength: 620nm) [22].
245

246 2.14 Outermembranepermeability

247 Bacteria in the logarithmic growth phase were collected by low-speed centrifugation, washed
248 twice with HEPES buffer (5mM HEPES + 5mM Glucose), resuspended, and then different
249 concentrations of PCA were added. A negative control group was also set up. After a 30-minute
250 treatment, 90μL of the sample was taken and added to a 96-well cell plate, followed by the
251 addition of 10μL of NPN for mixing. The fluorescence intensity was measured using an enzyme
252 labeling instrument (excitation wavelength: 350nm; emission wavelength: 420nm) [22].

253

254 2.15 Membrane depolarization assay

255 Bacteria in the logarithmic growth phase were collected by low-speed centrifugation, washed
256 twice with HEPES buffer (5mM HEPES + 20mM Glucose), and then resuspended. Subsequently,
257 10μL of KCL and 10μL of DisC3(5) were added to each sample tube, followed by gentle mixing
258 after a few minutes. Different concentrations of PCA were added to each sample tube, with a
259 negative control group set. The samples were treated for 30 minutes, and then transferred to a
260 96-well cell plate. Fluorescence intensity was measured using an enzyme labeling instrument
261 (excitation wavelength: 622nm; emission wavelength: 670nm) [23].

262

263 2.16 Bacterial metabolic viability experiment

264 Bacteria with a logarithmic growth phase were inoculated into a 96-well plate containing LB
265 medium at a concentration of 10^6 CFU/mL, with 200μL per well. Blank control group
266 (containing only LB medium) and positive control group (without drugs) were set up, and
267 different concentrations of PCA were added. The 96-well plate was incubated in a constant

268 temperature incubator at 37°C for 1 hour to allow the bacteria to adapt to the environment. 10μL
269 of alamarBlue reagent was added to each well to achieve a final concentration of 10%. The
270 96-well plate was incubated in a constant temperature incubator at 37°C for 4 hours to allow the
271 alamarBlue reagent to react with the bacteria. The absorbance (at a wavelength of 570nm) and
272 fluorescence intensity (excitation wavelength of 530nm, emission wavelength of 590nm) of each
273 well were measured using an enzyme-linked immunosorbent assay reader, and the relative
274 absorbance (subtracting the absorbance of the blank control group) and relative fluorescence
275 intensity (subtracting the fluorescence intensity of the blank control group) were calculated. The
276 metabolic activity of bacteria at different drug concentrations was evaluated using relative
277 absorbance or relative fluorescence intensity as indicators and compared with the positive control
278 group [24].
279
280 2.17 Untargeted metabolomics
281 According to the preliminary experimental results, the concentration of PCA was selected to study
282 the sub-inhibitory effect on CR-hvKP, and metabolomics analysis was conducted. The original
283 catechin with or without sub-inhibitory concentration was added to the logarithmic growth phase
284 CR-hvKP bacterial suspension and incubated at 37°C with constant shaking for 30 minutes. The
285 bacteria were then collected by centrifugation for 10 minutes, washed with sterile PBS, and stored
286 in liquid nitrogen. Metabolite samples were extracted from the intracellular and extracellular
287 samples using methanol/water (8:2, v/v). The intracellular and extracellular metabolite samples
288 were analyzed using liquid chromatography-mass spectrometry (LC-MS) and gas
289 chromatography-mass spectrometry (GC-MS), respectively. Data acquisition and processing were

290 performed using Xcalibur software, and data analysis and bioinformatics annotation were
291 conducted using MetaboAnalyst software [25].
292
293 2.18 G6PDH enzyme activity assay
294 Bacteria were cultured to the logarithmic growth phase and divided into two groups. One group
295 was treated with different concentrations of PCA, while the other group was treated with different
296 concentrations of glycerate-3P. After a 30-minute treatment, 1mL of extraction solution was added,
297 followed by ultrasonic disruption of the bacteria (200w, 3s ultrasound, 10s interval, repeated 30
298 times). The mixture was then centrifuged at 8000g for 10 minutes at 4℃, and the supernatant was
299 collected as the sample. In blank tubes and test tubes, 50μL of distilled water and 50μL of the
300 sample were added respectively, along with 950μL of working solution. 200μL of the mixture was
301 transferred to a 96-well plate, and the absorbance at 340nm was measured for both groups within
302 5 minutes. G6PDH activity (U/104cell) = 1.286×A2(300s)-A1(0s)[26].
303
304 2.19 Enzyme-linked immunosorbent assay
305 Dilute the capture antibody (1:100) in coating buffer (10mM phosphate buffer, pH 7.4) and add
306 100μL per well to a 96-well high-binding ELISA plate. Incubate overnight at 4℃. Wash the plate
307 3 times with phosphate-buffered saline containing 0.05% Tween 20 (PBST) for 5 minutes each
308 time, then remove excess liquid by blotting with absorbent paper. Block the plate with PBST
309 containing 1% bovine serum albumin (BSA), add 200μL per well, and incubate at room
310 temperature for 1 hour to block nonspecific binding sites. Wash the plate 3 times with PBST for 5
311 minutes each time, then remove excess liquid by blotting with absorbent paper. Dilute the

bacterial samples and standard solutions (known concentrations of the target protein) prepared by ultrasonic disruption in PBST containing 0.1% BSA, according to the predetermined gradient, and add 100μL per well. Incubate at room temperature for 2 hours to allow the target protein to bind to the capture antibody on the solid-phase carrier. Wash the plate 5 times with PBST for 5 minutes each time, then remove excess liquid by blotting with absorbent paper. Add the detection antibody (1:500) diluted in PBST containing 0.1% BSA to the plate, add 100μL per well, and incubate at room temperature for 1 hour to allow the detection antibody to bind to the immobilized target protein. The detection antibody is anti-human IgG antibody labeled with horseradish peroxidase (HRP), which can bind to different epitopes of the target protein. Wash the plate 5 times with PBST for 5 minutes each time, then remove excess liquid by blotting with absorbent paper. Add 100μL of TMB substrate to each well at room temperature and incubate in the dark for 15 minutes to allow HRP to catalyze the oxidation of TMB, resulting in a blue reaction product. The intensity of the reaction product is proportional to the concentration of the target protein. Add 50μL of stop solution (2M H2SO4) to each well to terminate the reaction and turn the reaction product yellow. Measure the absorbance (OD value) of each well at 450nm and plot a standard curve to calculate the concentration of the target protein in the samples [27].

2.20 Protein structure simulation and molecular docking

First, obtain the amino acid sequence of the target protein from the whole genome and use NCBI to perform a blast search for similar protein sequences for comparison. Then, use the multiple sequence alignment (MSA) to run the prediction script of Alphafold2 with default parameter settings, using the MSA as input, to obtain the three-dimensional structure model of the target

protein, as well as the confidence score (pLDDT) and distance error (dRMSD) for each residue. Afterwards, use Swiss-model to evaluate the quality of the protein structure model predicted by Alphafold2. Through the online interface of Swiss-model, calculate the structural similarity (TM-score) and root mean square deviation (RMSD) between the predicted model and template structure, as well as the global model quality estimation (GMQE) and local model quality estimation (QMEAN) scores for the predicted model [28-29].

Subsequently, AutoDock was used to study the interaction between protein models and small molecule ligands. First, AutoDockTools was used to preprocess the predicted proteins, including removing water molecules, adding hydrogen atoms, specifying active sites, assigning atomic charges, and adjusting flexibility. Then, MGLTools was used to convert the target protein and small molecule ligands into the pdbqt format required by AutoDock, and AutoGrid was used to calculate the grid potential field of the target protein. Next, AutoDock was used for molecular docking, setting parameters such as docking iterations, population size, crossover rate, and mutation rate, and selecting the docking conformation with the highest binding affinity. PyMOL was used for visualization and analysis. Firstly, the AutoDock plugin in PyMOL was used to load the target protein and docking conformations, and the sorting and filtering functions were used to select the conformation with the lowest binding energy as the optimal conformation. Then, the display and rendering functions in PyMOL were used to adjust the colors, transparency, surfaces, and outlines of the target protein and small molecule ligands to highlight their interactions. Finally, the measurement and annotation functions in PyMOL were used to label hydrogen bonds, van der Waals forces, and hydrophobic interactions between the target protein and small molecule ligands, and the three-dimensional images of the docking results were saved [30].

356

357 2.21 qRT-PCR validation

358 After overnight culture of the strain, total RNA was extracted according to the instructions of the
359 RNA extraction kit. The extracted bacterial RNA was used as a template for cDNA synthesis. The
360 reverse transcription reaction was performed according to the instructions of the reverse
361 transcription kit. 1000ng (1μg) of tRNA was prepared in a 20μl reaction system on ice. 4μl of 5×
362 PrimeScript RT Master Mix, 1000ng of RNA, and DEPC water were added to each well of an
363 8-well strip. The mixture was mixed using a vortex mixer. The reaction mixture was then
364 incubated at 37°C for 15 minutes for reverse transcription, followed by heat inactivation of the
365 reverse transcriptase at 85°C for 5 seconds, cooling at 4°C, and storage at -20°C for later use.
366 Using the CFX96 Real-Time system, PCR was performed in a 20μl reaction system containing 1μl
367 of cDNA, BPGM-F/R primers at a concentration of 10μmol/L, and 10μl of 2× FastFireqPCR
368 PreMix. The PCR program was set as follows: 95°C for 5 minutes; 40 cycles of 95°C for 5
369 seconds, 60°C for 30 seconds, and 72°C for 30 seconds; and a final extension at 72°C for 10
370 minutes. The relative expression level of the gene was calculated using the 2-ΔΔCt method with
371 the 16SrRNA gene as the reference gene [31].

372

373 2.22 Coenzyme Ⅱ NADP(H) Content Assay

374 Cultivate two bacteria to the logarithmic growth phase. Add different concentrations of PCA to
375 one sample for 30 minutes, and add different concentrations of 3-phosphoglyceric acid to the other
376 sample. Add 0.5mL of acidic extraction solution and 0.5mL of alkaline extraction solution to each
377 sample. Sonicate for 1 minute, then boil for 5 minutes, cool in an ice bath, and thaw at room

temperature. Centrifuge at 10,000g for 10 minutes, transfer the supernatant to another centrifuge tube, and add equal volumes of acidic extraction solution and alkaline extraction solution. Mix well and centrifuge again for 10 minutes. Transfer the supernatant to a new centrifuge tube for measurement. Measure the absorbance at 570nm [32].

2.23 Reactive Oxygen Species Assay

Bacteria were cultured to the logarithmic growth phase, centrifuged at 3500rpm for 10 minutes, washed and resuspended in PBS for 3 times. Then, the fluorescent probe DCFH-DA was added and incubated on a shaker at 37℃ for 30 minutes. After that, the samples were washed and resuspended in PBS for 3 times, divided into different tubes, and different concentrations of PCA were added. The tubes were placed in a 37℃ incubator for 30 minutes. The absorbance of each sample was measured using a fluorescence microplate reader (excitation wavelength: 488nm, emission wavelength: 525nm) [33].

2.24 Malondialdehyde (MDA) Content Assay

Bacteria were cultured to the logarithmic growth phase, and different concentrations of PCA were added for 30 minutes. The bacteria were then washed with sterile PBS and subsequently sonicated (200w, 3s on, 10s off, repeated 30 times). In blank tubes, standard tubes, and test tubes, 0.1mL PBS, 0.1mL standard solution, and 0.1mL sample were added, respectively. Then, 0.2mL MDA detection working solution was added and mixed. The mixture was heated at 100℃ for 15 minutes, followed by cooling to room temperature in a water bath. Subsequently, 200μL was aspirated into a 96-well plate and measured at 450nm [34].

400

401 2.25 Intracellular ATP assay

402 Bacteria were cultured to the logarithmic growth phase, and different concentrations of PCA were
403 added separately, with a negative control group set up. The cultures were placed on a shaker and
404 incubated at 37℃ for 30 minutes. After centrifugation, the supernatant was discarded and 200μL
405 of lysis buffer was added. The operation was carried out on ice, and then centrifuged at 4℃ and
406 12000g for 5 minutes. The supernatant was taken for measurement. Subsequently, 100μL of ATP
407 detection working solution was added to a 96-well plate, followed by the addition of 20μL of
408 sample or standard solution, with 3 replicates. Finally, the luminescence was measured using a
409 chemiluminescence luminometer [35].

410

411 2.26 Statistical analysis

412 The results are presented as the average of three independent experiments ± standard deviation.
413 One-way analysis of variance (ANOVA) and Student's t-test were used to detect any significant
414 differences between the treatments using Statplus ($p<0.05$) [36].

415

416 3 Results

417

418 3.1 In vitro antibacterial activity evaluation of natural plant monomer protocatechuic acid

419 Protocatechuic acid (PCA) is a phenolic acid compound that naturally occurs in many plants and
420 has various biological activities. It is currently mainly used in the fields of pharmaceutical
421 synthesis, organic intermediate synthesis, dye synthesis, and chemical reagents. It is also a core

raw material for various pharmaceutical products such as Erlotinib (anti-tumor drug), Liriodenine (sodium channel inactivation gate inhibitor), Meptifan hydrochloride (respiratory system drug), Corylifolin II (treatment of hepatitis B drug), Itopride hydrochloride (novel prokinetic drug), and Yimixing (anesthetic), etc. [37]. Although PCA also has antibacterial effects, the specific mechanism of action and targets are still unclear, so it has not been widely promoted as an antibacterial product. We determined the minimum inhibitory concentration (MIC) and minimum bactericidal concentration (MBC) of two strains of carbapenem-resistant hypervirulent Klebsiella pneumoniae (CR-hvKP) isolated from animal environments. The MIC of Meropenem against MEC19116-1 and FMEC20113-2 was 64ug/mL, while the MIC and MBC of PCA against MEC19116-1 and FMEC20113-2 were both 33μM, indicating that PCA has a certain antibacterial effect against CR-hvKP. Subsequently, we used a kinetic method to determine the inhibitory effect of PCA on CR-hvKP at different time points (0, 2, 4, 6, 8, 10, 12h). The results showed (Fig.1A) that the inhibitory effect of PCA on both strains increased with increasing concentration, showing concentration dependence. At a concentration of 1×MIC, PCA completely inhibited the growth of the strains. At a concentration of 1/2MIC, PCA slowed down the growth of the bacteria.To further observe the bacterial survival count of CR-hvKP under different drug concentrations, we used DAPI staining technique for fluorescence microscopy analysis. As shown in Fig.1B, we can see that the nuclei of bacteria in the normal culture (control group) exhibit uniform blue fluorescence, indicating stable DNA content and distribution. The nuclei of bacteria treated with PCA, on the other hand, show irregular blue fluorescence, indicating damage to DNA structure and integrity. Moreover, the blue fluorescence signal significantly decreases with increasing PCA concentration. These results suggest that PCA has a bactericidal effect on

CR-hvKP. To ensure the safety of PCA on the organism, we conducted a Hemolysis assay (Fig.1C) and found that the HC50 (μg/mL) of PCA on mammalian red blood cells is >20480 μg/mL, indicating that PCA is safe to use at antibacterial concentrations. In addition, we evaluated the potential development of resistance in CR-hvKP after long-term exposure to PCA. As shown in Fig.1D, after 20 generations of continuous passage at 1/2MIC concentration of PCA, the MIC remains stable, while the positive control drug tigecycline shows a 64-fold and 128-fold increase, respectively. This indicates that long-term use of the natural plant monomer PCA does not lead to a decrease in drug sensitivity of CR-hvKP, suggesting that PCA is more stable than antibiotics. Meanwhile, to evaluate whether PCA has a synergistic effect with antibiotics, we performed in vitro experiments on CR-hvKP using the checkerboard method and calculated the Fractional Inhibitory Concentration (FIC). Our experimental results (Fig.1E) show that when PCA is used in combination with meropenem, the MIC of both CR-hvKP strains is reduced by more than 4-fold. The median FIC is between 0.1 and 0.4, indicating a significant synergistic effect between PCA and meropenem. Therefore, the use of low concentrations of PCA can serve as an antibacterial adjuvant, providing a new possibility for the clinical treatment of CR-hvKP infections.

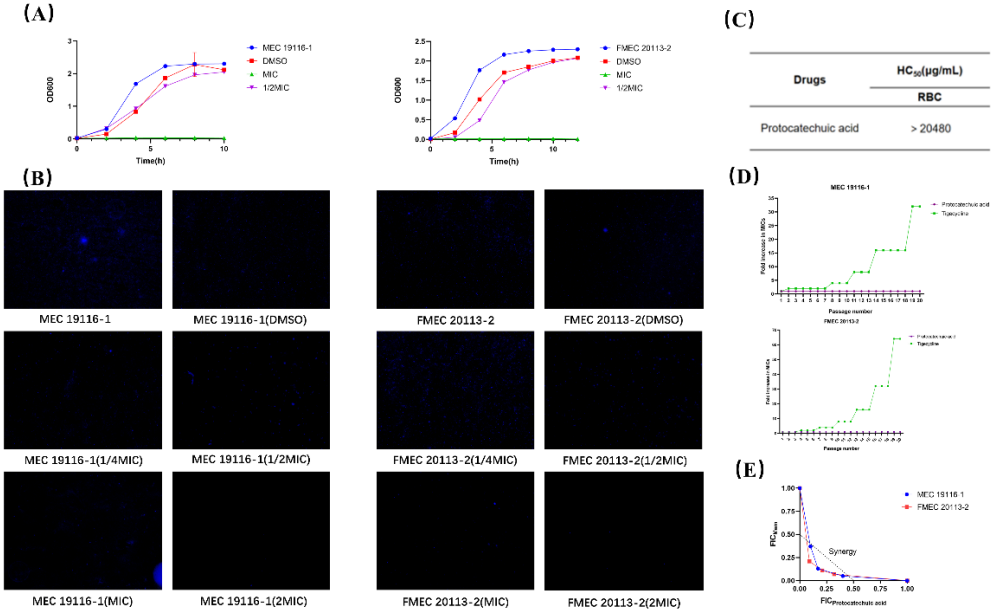

Fig.1. In vitro antibacterial activity evaluation of PCA. (A) Growth inhibition curve of CR-hvKP treated with PCA. (B) Bacterial DAPI staining after treatment with different concentrations of PCA. (C) HC50 (μg/mL) of PCA on mammalian red blood cells. (D) Potential development curve of drug resistance in CR-hvKP under continuous 20-generation drug treatment. (E) Synergistic study of PCA and meropenem using a checkerboard grid.

3.2 Inhibition of CR-hvKP biofilm by PCA at subinhibitory concentrations

Bacterial biofilms act as barriers that hinder the penetration and diffusion of antibiotics, reducing the effective concentration of antibiotics. The ability to form biofilms is closely related to the microbial physiological metabolism. In this study, we evaluated the biofilm formation of CR-hvKP treated with different concentrations of PCA. The Congo red agar plate method is a detection method that uses the principle of Congo red dye binding to the important components of biofilms, polysaccharides, to form black colonies for biofilm-positive strains and red colonies for

biofilm-negative strains [38]. Using this method (Fig.2A), we observed a significant decrease in the formation of positive colonies at 1/2MIC concentration of PCA, and the extracellular secretions were also significantly lower than the control group. Subsequently, we performed crystal violet staining of CR-hvKP biofilms (Fig.2B). PCA had a weak inhibitory effect on biofilms at low concentrations, but as the drug dosage increased, PCA showed a significant inhibitory effect on CR-hvKP biofilms ($p<0.01$), especially with an average inhibition rate of over 60% for MEC19116-1. EPS (extracellular polymeric substances) are high molecular weight natural polymers secreted by microorganisms into their environment, which have important effects on bacterial virulence, biofilm formation, and stability. The main components are polysaccharides, proteins, DNA, lipids, and other macromolecules [39]. Through the extraction and measurement of esp after PCA treatment (Fig.2C), it was found that PCA did not exhibit dose-dependent inhibition of eps at low concentrations, but instead caused compensatory increase. However, when the drug concentration exceeded a certain threshold, it could significantly inhibit esp ($p<0.001$). Overall, the inhibition of eps was consistent with the results of crystal violet staining. In addition, during the process of extracting esp from bacteria using a 6-well plate, we also found that the bacteria in the 6-well plate showed different color changes at different concentrations of PCA (Fig.2D) at 1/8MIC, 1/4MIC, 1/2MIC, MIC, and 2MIC drug concentrations. This may be due to the impact of PCA on bacterial metabolism [40].

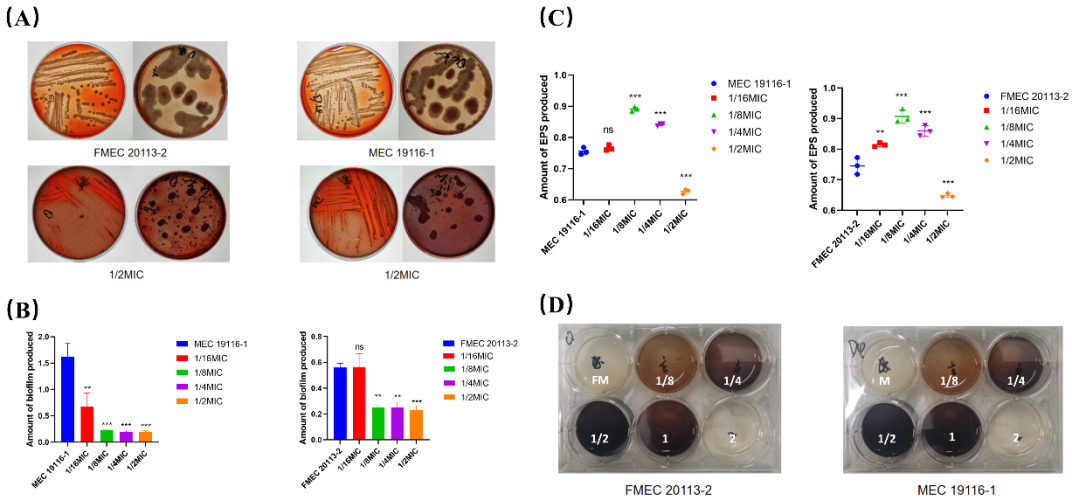

494

495 Fig.2. Evaluation of the inhibitory ability of sub-inhibitory concentration of PCA on CR-hvKP
496 biofilm. (A) Observation of bacterial biofilm in control group and sub-inhibitory concentration
497 PCA treatment group. (B) Crystal violet staining of biofilm after treatment with different
498 concentrations of PCA under sub-inhibitory conditions. (C) Measurement of extracellular
499 polymeric substances. (EPS) after treatment with different concentrations of PCA under
500 sub-inhibitory conditions. (D) Color change of bacterial culture medium under different
501 concentrations of PCA treatment (numbers in the figure represent drug concentrations). Values are
502 presented as mean ± SD. ns represents (P>0.05), * represents (P<0.05), ** represents (P<0.01),
503 *** represents (P<0.001), all compared to the control group.

504 3.3 The effect of subinhibitory concentration of PCA on the cell membrane of CR-hvKP

505

506 The bacterial cell membrane is the first line of defense against antibiotic resistance in bacteria.
507 Bacteria can reduce the entry of antibiotics by changing the permeability of the cell membrane,
508 thereby developing resistance. This change can be a defect or reduction in the expression of pore
509 proteins, or a change in the membrane potential [41]. In addition, the relationship between the

510 bacterial cell membrane and metabolism is a complex and interesting topic. Due to the rich
511 enzyme system present on the membrane, it serves as a site for many important metabolic
512 activities in bacteria [42]. The cell membrane is also closely related to bacterial quorum sensing
513 and biofilm formation. Quorum sensing signal molecules freely diffuse or actively transport
514 through the bacterial cell membrane, bind to receptors inside and outside the cell, and trigger
515 downstream signaling pathways as well as the formation and maintenance of biofilms [43-44]. In
516 this study, we first observed the morphology of the bacterial cell membrane after treatment with
517 sub-inhibitory concentration of PCA using scanning electron microscopy (Fig.3A). We found that
518 the cell membrane of FMEC20113-2 became rough and uneven under PCA treatment, while the
519 control group maintained a smooth and uniform morphology. The cell membrane of MEC19116-1
520 even showed damage and leakage of cellular contents. This indicates that PCA has a significant
521 damaging effect on the cell membrane of CR-hvKP and affects membrane permeability. The
522 permeability of the bacterial cell membrane has a bidirectional impact on bacterial metabolism.
523 Normal metabolic activities require stable membrane permeability to ensure the exchange of
524 substances between the inside and outside of the cell and the stability of the internal environment.
525 On the other hand, bacterial metabolism can also affect changes in cell membrane permeability by
526 altering the composition and structure of the cell membrane or producing substances that affect
527 membrane permeability [45]. Therefore, in the following study, we evaluated the inner membrane
528 permeability using the non-permeable nucleic acid binding dye PI, which can only enter the cell
529 through a damaged cell membrane and bind to DNA or RNA, emitting red fluorescence [46]. By
530 measuring the fluorescence intensity (Fig.3B), we found that the fluorescence value after PCA
531 treatment increased with the drug concentration, indicating a dose-dependent positive correlation

between inner membrane permeability and PCA ($P<0.01$). Furthermore, we used a fluorescent dye NPN (1-N-phenylnaphthylamine) to measure the outer membrane permeability of CR-hvKP. NPN can dissolve in the lipid bilayer but cannot penetrate intact bacterial outer membranes. When the bacterial outer membrane is damaged, NPN can enter the periplasmic space of the bacteria and interact with hydrophobic molecules, emitting fluorescence, reflecting changes in bacterial outer membrane permeability [47]. As shown in (Fig.3C), the fluorescence intensity after PCA treatment increased with the drug concentration, indicating a dose-dependent positive correlation between outer membrane permeability and PCA ($P<0.001$). As for why the fluorescence intensity decreased at MIC concentration, we believe that PCA at MIC concentration caused obvious damage to the outer membrane of the bacteria, causing it to detach from the cell wall, and the hydrophobic environment of the periplasmic space no longer existed, resulting in a decrease in fluorescence intensity [48]. Changes in membrane permeability also affect membrane potential. Membrane potential is a crucial source of free energy for bacteria and can affect bacterial signal transduction, stress regulation, and antibiotic resistance. For example, the bacterial respiratory chain and ATP synthase are located on the cell membrane, and they require membrane permeability to maintain membrane potential and proton gradient for energy conversion and utilization [41]. In this study, we measured the $\Delta\psi$ of the cell membrane using the fluorescence DiSC3(5) method [49]. DiSC3(5) is a membrane potential-sensitive probe that aggregates in the phospholipid bilayer and causes self-quenching of the dye. When the membrane is depolarized, the potential dissipates, and diSC3(5) is released into the solution, causing an increase in fluorescence, which is proportional to the degree of membrane potential decrease [50]. As shown in (Fig.3D), the fluorescence intensity increased with the drug concentration after PCA treatment

554 (P<0.05), indicating that the Δψ depolarization of the CR-hvKP cell membrane is affected by PCA.

555 In summary, the results of the cell membrane study further illustrate the impact on bacterial

556 activity and metabolism.

557

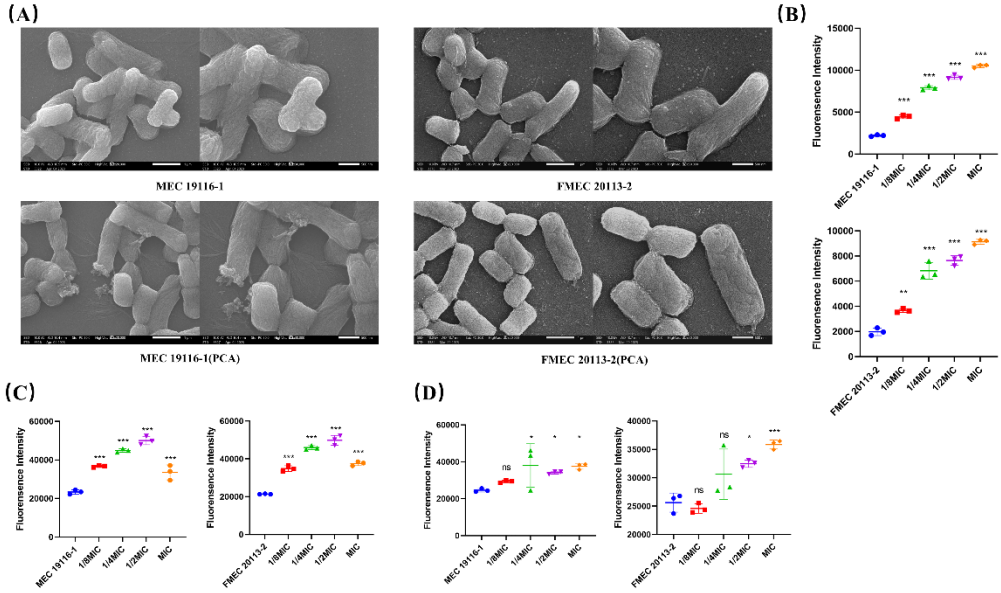

558

559 Fig.3. The effect of subinhibitory concentrations of PCA on the bacterial cell membrane of

560 CR-hvKP as studied by PCA. (A) Morphological observation of bacteria in the control group and

561 PCA treatment group. (B) Intracellular membrane permeability after treatment with different

562 concentrations of PCA under subinhibitory conditions. (C) Extracellular membrane permeability

563 after treatment with different concentrations of PCA under subinhibitory conditions. (D) Cell

564 membrane Δψ after treatment with different concentrations of PCA under subinhibitory conditions.

565 Values are presented as mean ± SD. In the figure, ns indicates (P>0.05), * indicates (P<0.05), **

566 indicates (P<0.01), *** indicates (P<0.001), all compared to the control group.

567

568 3.4 The effect of subinhibitory concentration of PCA on bacterial metabolism

569

As mentioned above, the steady state of the cell membrane has a bidirectional effect on bacterial metabolism. In order to study the effect of PCA on bacterial metabolic status, we used AlamarBlue to detect the bacterial viability and metabolic activity after drug treatment. During normal metabolic processes, the intracellular environment of bacteria changes from an oxidative environment to a reducing environment. The active component of AlamarBlue, resazurin, is a non-toxic and membrane-permeable blue dye. After being taken up by the cells, it is reduced by metabolic intermediates, and the reduced product, resorufin, appears pink and exhibits strong fluorescence [51]. In this study (Fig.4A), we found that the fluorescence intensity of bacteria decreased after PCA treatment ($P<0.05$). With increasing drug concentration, a color different from pink was observed, indicating that the drug reduced the metabolic activity and reducing ability of the bacteria.

Subsequently, we used metabolomics to analyze the bacterial metabolic activity of CR-hvKP treated with PCA, in order to gain a more comprehensive understanding of how PCA affects CR-hvKP and its underlying mechanisms. Metabolomic analysis was performed using a UPLC-Q-TOF/MS system and multivariate statistical analysis to analyze the perturbation of metabolite profiles in the cells of two CR-hvKP strains treated with PCA. Differential metabolites (DMs) were selected based on the OPLS-DA model, which provided convincing parameters with high R2Y and Q2Y values. Both the control group and the treatment group showed distinct clustering behavior. All replicates of each group were assigned to the same cluster, confirming the observed differences in metabolite profiles between the control and treatment groups (Fig.4B).As shown in Fig. 4C, in the FMEC20113-2 group, compared to the control group, 2029 significantly

592 altered metabolites were identified, including 1104 upregulated and 661 downregulated. Similarly,
593 in the MEC19116-1 group, compared to the control group, 2239 significantly altered metabolites
594 (VIP>1, P<0.05) were identified, including 957 upregulated and 598 downregulated. Meanwhile,
595 we presented the shared differential metabolites of the two bacterial groups in a Venn diagram
596 (Fig. 4D).
597
598 Finally, we performed KEGG enrichment analysis to show the significantly enriched pathways in
599 two groups of bacteria after PCA treatment, and analyzed the overall changes in these metabolic
600 pathways based on differential abundance scores (Fig. 4E and F). We found that most of these
601 co-enriched metabolic pathways showed downregulation. Through analysis, we found that the
602 metabolic pathways including "Cysteine and methionine metabolism", "Biosynthesis of various
603 antibiotics", "Aminosugar and nucleotide sugar metabolism", "Caffeine metabolism",
604 "Biosynthesis of nucleotide sugars", and "Biosynthesis of cofactors" were strongly associated with
605 the Pentose phosphate pathway (PPP). For example, in the pathways of "Biosynthesis of
606 nucleotide sugars" and "Aminosugar and nucleotide sugar metabolism", bacteria can generate
607 ribose-5-phosphate from glucose or other hexose sugars through the PPP pathway, and then
608 convert it into various aminosugars and nucleotide sugars through different transferases [52-54].
609 In the pathway of "Cysteine and methionine metabolism", bacteria reduce inorganic sulfur to
610 hydrogen sulfide using NADPH provided by the PPP pathway, and then react with serine or
611 methionine to generate cysteine or methionine [55]. In addition, other significant metabolic
612 pathways were related to amino acid metabolism, which requires amino acids as precursors and
613 depends on ribose-5-phosphate produced by the PPP pathway [54]. In summary, the PPP pathway

614 is a key influencing pathway for drug response, as it is closely related to other significantly
615 changed bacterial metabolic pathways. It can provide important metabolic intermediates such as
616 ribose-5-phosphate and NADPH, and participate in the synthesis and regulation of various
617 biomolecules in these pathways. When the PPP pathway is affected, these associated metabolic
618 pathways show downregulation.
619
620 Therefore, we analyzed the changes in the metabolites of the pentose phosphate pathway (PPP) in
621 two groups of bacteria after PCA treatment. The PPP, also known as the pentose phosphate
622 pathway, is a metabolic pathway in bacteria that can produce ribose-5-phosphate and NADPH in
623 cells, which are essential for the synthesis of biomolecules such as nucleic acids and coenzymes
624 [54]. Moreover, the PPP affects the energy metabolism of bacteria by regulating glycolysis and the
625 citric acid cycle [56]. The PPP consists of two stages: oxidative and non-oxidative. In (Fig.4G), it
626 can be seen that the oxidative stage of the PPP starts with β-D-glucose-6-phosphate, which is an
627 intermediate product of glycolysis and the first substrate of the PPP. It is oxidized by
628 glucose-6-phosphate dehydrogenase (G6PDH) to D-glucono-1,5-lactone-6P, while reducing
629 NADP+ to NADPH. This is the first reaction of the PPP and the rate-limiting reaction, which
630 determines the activity of the PPP. D-glucono-1,5-lactone-6P is hydrolyzed by a hydrolase to
631 D-gluconate-6P, also known as 6-phosphogluconate, which is an intermediate product of the PPP.
632 6-phosphogluconate is oxidized by 6-phosphogluconate dehydrogenase (6PGDH) to
633 D-ribulose-5P, while reducing NADP+ to NADPH. This is the second reaction of the oxidative
634 stage of the PPP and the last reaction of the oxidative stage, which produces two NADPH and one
635 5-phosphoribose. The non-oxidative stage of the PPP starts with D-ribulose-5P in the top right

636 corner, which is the last product of the oxidative stage and the first substrate of the non-oxidative
637 stage [56]. It is isomerized to D-ribose-5P by ribose-5-phosphate isomerase (RPI). D-ribose-5P is
638 an important carbon skeleton that can participate in various biological processes such as the
639 synthesis of nucleic acids and coenzymes, as well as carbon metabolism [57].
640
641 Through metabolomics analysis (Fig.4G), it was found that the glycerate-3P in bacteria showed a
642 significant upregulation after treatment with both drugs. Glycerate-3P is a common molecule in
643 biological cells and is an intermediate product of the glycolysis (EMP) pathway. It is usually used
644 as a raw material for the synthesis of other organic molecules such as glucose, nucleic acids, and
645 fatty acids [58]. When the concentration of glycerate-3P is too high, it can have a certain impact
646 on the bacteria's PPP pathway. This is because excessive glycerate-3P can reduce the flux of the
647 PPP pathway. The excessive accumulation of this intermediate product will compensatorily
648 change the activity and expression of the rate-limiting enzyme in the pathway, which is
649 glucose-6-phosphate dehydrogenase (G6PDH) in the PPP pathway. This compensatory
650 mechanism eventually evolves into a stress response, where G6P is blocked from entering the
651 reaction for a long time, severely slowing down the oxidative stage of the PPP pathway, resulting
652 in a decrease in NADPH production, an increase in intracellular oxidative stress, and damage to
653 DNA, proteins, and lipids, ultimately leading to apoptosis or necrosis [59]. NADPH is an
654 important reducing agent that participates in biosynthesis and antioxidant processes. On the other
655 hand, due to the slowdown of the oxidative stage of the PPP, the generation of ribose-5-phosphate
656 will decrease, further affecting the synthesis of nucleic acids and coenzymes, inhibiting bacterial
657 growth and metabolism [57]. For example, as observed in (Fig.4G), the significant downregulation

658 of D-ribose-1P, which is converted from D-ribose-5P (a type of 5-phosphoribose) catalyzed by
659 ribose-phosphate isomerase (RPE), is a result of the inhibition of the PPP pathway.
660
661 We speculate that pyruvic acid (PCA), as an organic acid, can enter bacterial cells and affect the
662 bacterial EMP, thereby inhibiting bacterial growth and metabolism. In glycolysis (Fig.4H),
663 glucose is converted to glyceraldehyde-3-phosphate (G3P), which is then phosphorylated and
664 converted to 1,3-diphosphoglycerate (1,3-DPG). Subsequently, under the action of
665 phosphoglycerate kinase (PGK), 1,3-DPG is converted to glycerate-3-phosphate (G3P), and then
666 under the action of phosphoglycerate mutase (PGAM), G3P is converted to glycerate-2-phosphate
667 (G2P), finally leading to the production of pyruvate [58]. It is worth noting that the reactions in
668 this stage are reversible and adjusted by the relative concentration of intermediate products, so
669 G3P can be converted between different pathways of EMP to maintain normal metabolism [58].
670 Therefore, if PCA inhibits the activity of PGAM, G3P cannot be converted to G2P, and even G2P
671 may be downregulated. However, in this case, bisphosphoglycerate mutase (BPGM) can catalyze
672 the conversion of G3P to glycerate-2,3-phosphate (G2,3P), thereby continuing to participate in the
673 metabolic process and ensuring the steady progress of EMP. This is a compensatory mechanism of
674 bacteria. Although the gene expression level of BPGM in Klebsiella pneumoniae is relatively low
675 and only induced when the pathway is abnormal, it can alleviate the toxic effects caused by the
676 excessive accumulation of G3P [60-61]. However, when BPGM is also inhibited by PCA, the
677 concentration of G3P will continue to rise because it cannot be effectively utilized or cleared. This
678 further leads to the blockage of the EMP pathway itself and the pentose phosphate pathway,
679 resulting in metabolic disorders.

The mainstream metabolic pathway in most microorganisms is the EMP pathway, but few microorganisms rely solely on the EMP pathway for metabolism, mostly through the combined action of the EMP and PPP pathways. Based on the analysis of metabolomics reports, we found that PCA mainly inhibits the action of EMP and simultaneously blocks the PPP pathway in CR-hvKP, leading to an imbalance in the redox state of the bacterial body and disruption of energy metabolism, as well as inhibition of biofilm function and changes in membrane permeability.

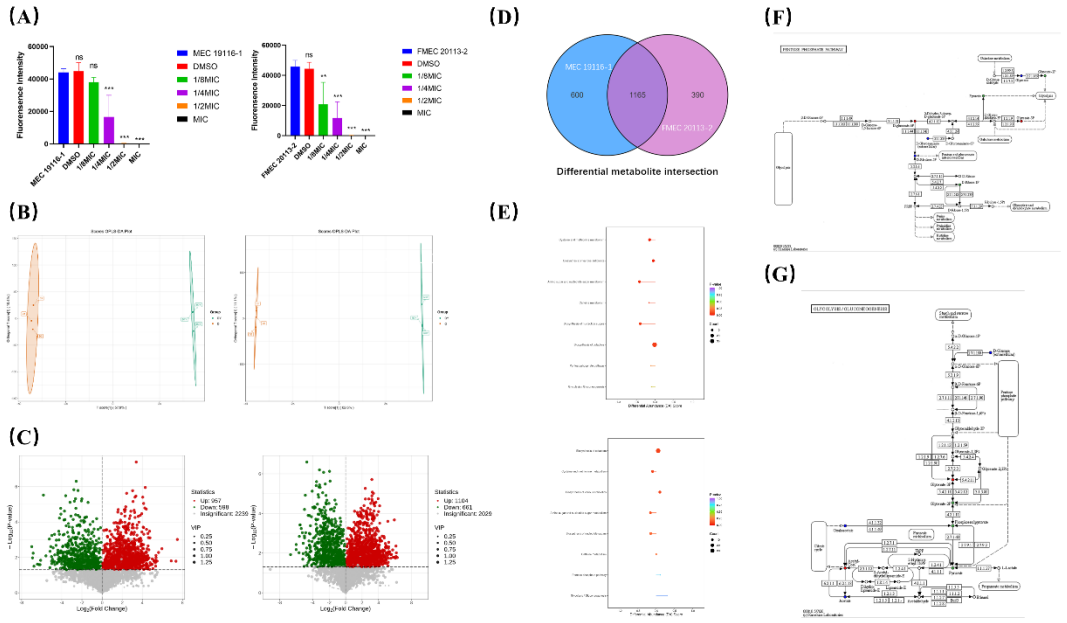

Fig.4. The effect of subinhibitory concentrations of PCA on bacterial metabolism as determined by PCA. (A) AlamarBlue assay measuring the metabolic activity of CR-hvKP after PCA treatment. (B) Differential metabolite profiles after PCA treatment at subinhibitory concentrations ($P<0.05$). (C) Volcano plot of differential metabolites; significantly upregulated and downregulated metabolites are shown in red and green, respectively, while non-significant differentially expressed metabolites are shown in gray. (D) Venn diagram of differential metabolites between

the two groups. (E) KEGG enrichment analysis of differential metabolites, showing the most significantly enriched pathways. (F) Changes in the pentose phosphate pathway and associated metabolites; significantly upregulated and downregulated metabolites are shown in red and green, respectively. (G) Changes in the glycolysis pathway and associated metabolites; significantly upregulated and downregulated metabolites are shown in red and green, respectively.

3.5 Changes in key metabolic enzymes

To validate the results obtained in metabolism, we first detected the activity of G6PDH after PCA treatment of bacterial cells, as shown in (Fig.5A). PCA stimulated bacterial compensation at low concentrations, leading to an increase in G6PDH activity. In this case, the flux of the pentose phosphate pathway would increase, the NADPH/NADP+ ratio would rise, and thus meet the requirements for cellular biosynthesis and resistance to oxidative stress under drug stimulation. However, as the concentration of PCA increased, this compensatory mechanism could not be maintained, resulting in a decrease in G6PDH activity ($P<0.05$). At the same time, we added exogenous glycerate-3P and retested the activity of G6PDH, as shown in (Fig.5B). When 0.2μM and 0.5μM were added, the activity of G6PDH decreased to half of the original level. However, when we added >1μM glycerate-3P, G6PDH activity decreased significantly ($P<0.001$). This indicates that glycerate-3P does indeed inhibit the function of G6PDH under conditions of excessive accumulation, as we expected.

Meanwhile, we also detected the activity of PGAM enzyme through ELISA, and the results are

718 shown in (Fig.5C). As the concentration of PCA increases, the activity of PGAM decreases,
719 indicating that PCA indeed has an inhibitory effect on PGAM activity, and this effect shows a
720 dose-dependent relationship ($P < 0.05$). In order to explore the interaction between PCA and
721 PGAM, we performed molecular docking between PCA and PGAM. In Klebsiella pneumoniae,
722 PGAM is mainly encoded by gpma and gpmb. Although the proteins encoded by gpma and gpmb
723 have the same enzymatic activity, they have different functional domains, so we docked both of
724 them. In our previous study, we obtained the whole genome sequence of FMEC20113-2 and
725 obtained the amino acid sequence information of gpma and gpmb from it. Then we simulated their
726 protein structures using Alphafold2 and evaluated the quality of protein structure modeling using
727 Swiss-model (Fig.5D) to obtain the most suitable protein structure. Based on this, we employ
728 Autodock molecular docking software to integrate PCA with proteins, discernring that both PCA
729 and the proteins encoded by gpma and gpmb exhibit robust affinity for attachment.. Finally, we
730 used pymol software to display the key amino acids of the two proteins binding with PCA and
731 analyzed their interactions. As shown in (Fig.5E), PCA exerts its inhibitory effect on activity by
732 binding to the amino acid residues GLU-125, THR150, and THR151 of gpma, and by binding to
733 the amino acid residues LEU337, GLY342, and SER343 of gpmb. The main interaction between
734 them is through hydrogen bonding, which affects the function of the target protein.
735
736 In the previous discussion, we mentioned that bacteria can convert excessive glucerate-3P through
737 compensatory expression of BPGM. Therefore, in this study, we simultaneously detected the
738 activity and content of BPGM enzyme, as shown in (Fig.5F). Although the activity of BPGM
739 fluctuated slightly under the influence of the drug, it remained at a low level of activity regardless

740 of the drug concentration (P>0.05). Therefore, PCA may not have a significant impact on the
741 activity of BPGM. Since the expression level of the BPGM gene itself is low in microorganisms,
742 we suspect that the inhibitory effect of PCA occurs during its transcription process. Therefore, we
743 conducted RT-qPCR experiments (Fig.5G) and found that compared to the negative group treated
744 with DMSO, PCA significantly downregulated the transcription of bpgm, and the inhibitory effect
745 of PCA was more pronounced in the MEC19116-1 group (P<0.001). As for the upregulation
746 observed in the DMSO group, this may be due to bacterial compensation caused by environmental
747 changes.
748
749 In conclusion, as we obtained in the metabolomics analysis, the upregulation of the signature
750 metabolite glycerate-3P is due to the inhibition of the EMP pathway. The accumulation of this
751 intermediate product will compensatorily affect the rate-limiting enzyme of the PPP pathway,
752 ultimately leading to a decrease in the activity and expression of G6PDH, resulting in a significant
753 inhibition of the PPP metabolic pathway and causing endogenous oxidative stress.
754

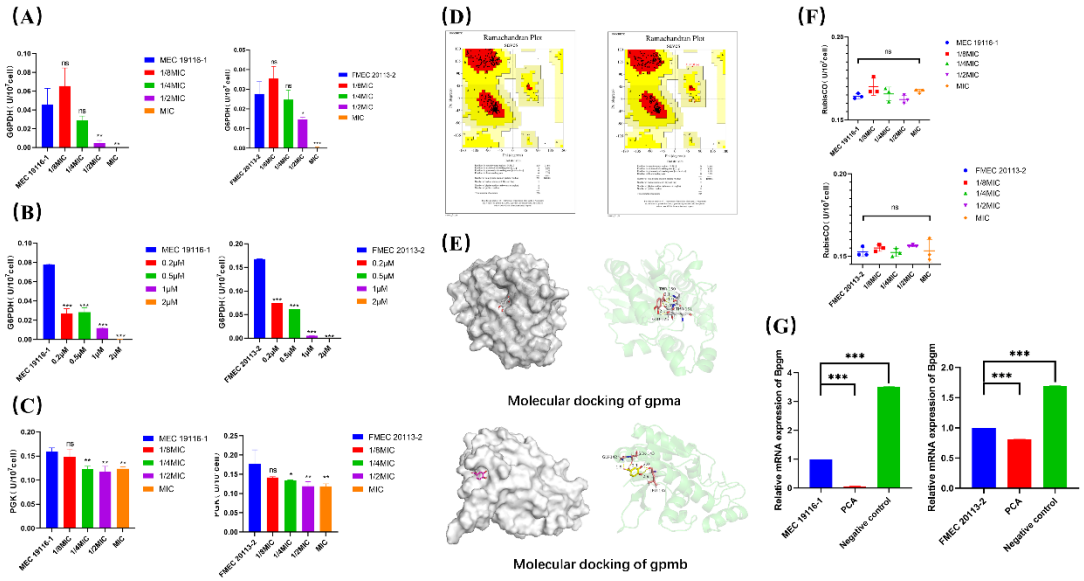

Fig.5. The effect of subinhibitory concentration of PCA on key metabolic enzymes. (A) Effect of subinhibitory concentration of PCA on G6PDH activity. (B) Effect of exogenously added glycerate-3P at different concentrations on G6PDH activity. (C) Effect of PCA on PGAM enzyme activity. (D) Quality assessment of 3D structure modeling of gpma and gpmb proteins. (E) Molecular docking simulation of PCA with gpma and. (F) Effect of PCA on BPGM enzyme activity. (G) Transcriptional effect of PCA on BPGM at subinhibitory concentration. Values are presented as mean ± SD. In the figure, ns indicates (P>0.05), * indicates (P<0.05), ** indicates (P<0.01), *** indicates (P<0.001), all compared to the control group.

3.6 Endogenous Oxidative Stress in Bacteria

The pentose phosphate pathway (PPP) is a key pathway for regulating the NADPH/NADP+ balance, ensuring the redox balance inside bacterial cells. In addition, NADPH, as an important reducing agent, can provide reducing power to drive various cellular synthesis reactions. For example, NADPH can participate in fatty acid synthesis by extending the fatty acyl chain through

771 the reduction of fatty acyl-ACP reductase (FASR). NADPH can also participate in cholesterol
772 synthesis by generating methylglutaconyl-CoA through the reduction of HMG-CoA reductase
773 (HMGR). NADPH is also involved in nucleotide synthesis by generating deoxyribonucleotides
774 through the reduction of nucleotide reductase (NR). NADPH can also participate in the synthesis
775 of amino acids such as proline, tryptophan, and tyrosine. NADPH is also an important signaling
776 molecule that can affect cell signaling by regulating intracellular calcium levels, nitric oxide
777 synthase (NOS) activity, and oxidative stress response. Some studies have shown that NADPH
778 can regulate biofilm formation by affecting the c-di-GMP levels inside bacteria. c-di-GMP is a
779 widely distributed second messenger in bacteria that can regulate bacterial motility, adhesion, and
780 biofilm formation. Additionally, NADPH is also an important antioxidant that can eliminate
781 reactive oxygen species (ROS) by reducing molecules such as glutathione (GSH) and thioredoxin
782 (Trx). Therefore, when the PPP pathway is inhibited, NADPH is downregulated, resulting in a
783 decrease in the bacteria's antioxidant capacity and susceptibility to oxidative damage. In this study,
784 we measured the intracellular NADPH/NADP+ ratio after PCA treatment, as shown in Figure 6A.
785 When PCA was used at a concentration below 1/2MIC, the NADPH/NADP+ ratio significantly
786 decreased. This is because the inhibition of glucose-6-phosphate dehydrogenase (G6PDH)
787 prevents the reduction of NADP+ to NADPH. As the drug concentration increases, the synthesis
788 of NADP+ is also affected, for example, by inhibiting the activity of NAD kinases (NADKs),
789 leading to a decrease in NAD+ conversion to NADP+. In this case, the NAD+ content also
790 decreases, resulting in an increase in the NADPH/NADP+ ratio. Therefore, combined with
791 previous studies such as the significant downregulation of amino acid and nucleotide synthesis in
792 metabolomics, as well as the inhibition of biofilm formation, it is evident that the alteration of the

NADPH/NADP+ balance severely affects the growth and function of CR-hvKP.

Based on this, we also determined the levels of bacterial ROS and malondialdehyde (MDA). ROS are a type of highly reactive free radicals that can damage bacterial structures such as membranes, proteins, and nucleic acids, leading to bacterial dysfunction and death [66]. MDA is the main product of lipid peroxidation and a commonly used indicator to measure the degree of lipid oxidative damage. When the intracellular ROS levels are high, unsaturated fatty acids react with ROS to produce a series of peroxides and MDA as end products [67]. The results, as shown in (Fig. 6B and C), indicate a positive correlation between the concentration of PCA and the levels of bacterial intracellular ROS and MDA ($P < 0.001$). This result is consistent with the changes in NADPH/NADP+ and further supports the notion that the disruption of bacterial PPP metabolism is the cause of bacterial oxidative stress.

Both oxidative stress-induced damage to the respiratory chain and changes in cell membrane potential, as well as inhibition of the EMP pathway, can reduce the decline of intracellular ATP, affecting energy balance and bacterial function. Therefore, we also measured the changes in intracellular ATP levels, as shown in (Fig.6D). At low concentrations, PCA does not affect the intracellular ATP levels, but instead increases its content. This is due to the compensatory effect of low-dose drug stimulation on bacteria. However, as the concentration increases, due to the destructive and inhibitory effects of PCA on the respiratory chain and EMP, intracellular ATP levels decrease.

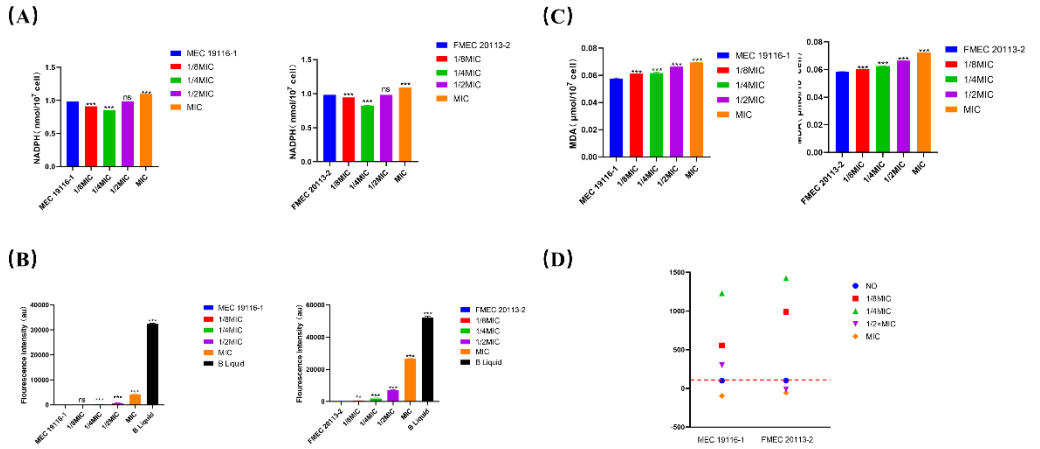

Fig6. The effect of subinhibitory concentration of PCA on the redox state of bacteria as analyzed by PCA. (A) The effect of subinhibitory concentration of PCA on intracellular NADPH/NADP+ ratio. (B) The effect of subinhibitory concentration of PCA on intracellular ROS levels. (C) The effect of subinhibitory concentration of PCA on intracellular MDA levels. (D) The effect of subinhibitory concentration of PCA on intracellular ATP levels.Values are presented as mean ± SD. In the figure, ns indicates (P>0.05), * indicates (P<0.05), ** indicates (P<0.01), *** indicates (P<0.001), all values compared to the control group.

4. Discussion

In the context of the widespread spread of drug-resistant bacteria, the treatment of antibiotics has become difficult, and increasing the dosage can lead to a vicious cycle, with bacteria becoming less and less sensitive to antibiotics or even developing new resistance [68]. People have begun to explore the possibility of using bioactive molecules from natural plant sources as antibacterial drugs and antibacterial enhancers [69-70]. Protocatechuic acid is a polyphenolic compound found in various natural plants. Previous studies have focused on its excellent antioxidant properties, as

well as its anti-inflammatory and anticancer effects in the body [71-72]. Considering that PCA is an important raw material that has been used in pharmaceutical synthesis for a long time and has a high level of safety, this study investigated the antibacterial activity of PCA against drug-resistant bacteria and its related mechanisms. Based on antibacterial tests, we found that PCA can inhibit the growth of CR-hvKP at lower concentrations. In addition, PCA also has a synergistic effect with the carbapenem antibiotic meropenem. Continuous treatment with PCA does not induce resistance in CR-hvKP compared to other antibiotics. Since subinhibitory concentrations of PCA can synergistically inhibit bacteria with meropenem, we also studied the inhibitory effect of PCA on CR-hvKP biofilms and its impact on cell membranes at subinhibitory concentrations. The results showed that besides being used as an antibacterial drug on its own, PCA can also act as an antibacterial enhancer by inhibiting biofilm formation and altering membrane permeability at low concentrations, making it a potential candidate drug against drug-resistant bacteria.

The metabolic homeostasis of the internal environment is crucial for the function and growth of bacteria [73]. Key enzymes in metabolic pathways and secondary metabolites are promising targets for screening candidate antibacterial agents [74]. For example, research has targeted key enzymes in the bacterial folate metabolism pathway to design folate antagonist antibacterial drugs, such as inhibitors of dihydrofolate reductase (DHFR) [75]. There are also studies that use metabolomics-based methods to explore the interaction mechanisms between antibiotics and bacteria, thereby screening for more novel antibiotics [76]. Due to the antibacterial activity of certain secondary metabolites, such as pyocyanin (PYO) in Pseudomonas aeruginosa and pyocyanin in Staphylococcus aureus [77], we can also develop antibacterial drug adjuvants

854 targeting the metabolites themselves. Since there is a bidirectional influence between bacterial cell
855 membrane and bacterial metabolic activity [42][45], the function of biofilms is also regulated by
856 bacterial metabolism [78-79]. Therefore, to gain a deeper understanding of the biological
857 mechanism of PCA on CR-hvKP, metabolomics methods were used to describe the major changes
858 in the biological processes of CR-hvKP after PCA treatment. The results showed that PCA
859 interfered with multiple biological pathways related to amino acid metabolism in CR-hvKP,
860 considering that the production of amino acids mainly relies on the precursors provided by the
861 PPP pathway. We speculate that the main metabolic pathways disrupted by PCA are the PPP
862 pathway and the closely related glycolysis pathway.
863
864 The main pathway for microbial energy metabolism is the glycolysis pathway, in which bacteria
865 break down sugars into pyruvic acid or other organic acids and generate energy [80]. There are
866 four main pathways for bacterial glycolysis: EMP, HMP, ED, and WD. Most microorganisms rely
867 on the combined action of EMP and HMP [81]. The EMP pathway is the most common glycolysis
868 pathway and the first stage of cellular respiration. It consists of 10 steps, converting 1 molecule of
869 glucose into 2 molecules of pyruvic acid, and producing 2 molecules of ATP and 2 molecules of
870 NADH [82]. The HMP pathway, also known as the PPP pathway mentioned earlier, is a pentose
871 phosphate pathway. It degrades 6-phosphogluconate as a substrate and is divided into two stages:
872 oxidative and non-oxidative stages. This pathway can provide reducing power NADPH and
873 carbon skeletons for biosynthesis, and can also connect with the EMP pathway to expand the
874 range of carbon sources utilization [83]. Studies have shown that EMP and PPP are interdependent
875 and mutually influenced. For example, the product of glycolysis, pyruvic acid, can enter the

tricarboxylic acid cycle, and the intermediate products of the tricarboxylic acid cycle can enter the pentose phosphate pathway. They collectively generate energy, reducing power, and precursor substances in the cytoplasm, and regulate their own activity and flow according to the needs of the cytoplasm and changes in the environment [84]. The metabolomics results of this study indicate that the metabolite 3-phosphoglyceric acid in the EMP pathway is significantly upregulated. The abnormal accumulation of this intermediate metabolite may lead to blockage of the PPP pathway, resulting in a series of cellular functional disorders. For example, the accumulation inhibits downstream reactions, reduces the production of NADPH, leading to oxidative-reductive imbalance in the cell; reduces the production of R5P, affecting nucleic acid synthesis; reduces the production of GAP, reducing energy supply, etc. [85-87]. In this study, we found that the activity of the rate-limiting enzyme G6PDH in the PPP pathway is affected by the intermediate metabolite 3-phosphoglyceric acid, and the metabolic disorder of 3-phosphoglyceric acid is the result of the inhibition of the key enzyme PGAM by PCA. We verified this result through molecular docking. In addition, when 3-phosphoglyceric acid is metabolically abnormal, microorganisms compensatorily express BPGM to alleviate this situation [88]. We found through enzyme-linked immunosorbent assay and real-time fluorescence quantitative PCR that PCA significantly downregulates the expression of BPGM. These results indicate that PCA inhibits protein activity by hydrogen bonding with PGAM amino acid residues, and also inhibits the expression of the bypass pathway BPGM, leading to abnormal accumulation of the key metabolite 3-phosphoglyceric acid. This accumulation not only affects the normal operation of the EMP pathway but also negatively inhibits the PPP pathway, ultimately leading to the comprehensive shutdown of microbial energy metabolism.

It is worth noting that the inhibition of the pentose phosphate pathway (PPP) alters the redox state of bacteria, leading to endogenous oxidative stress. This is because the PPP is the main source of NADPH, and the balance between NADPH and NADP+ is crucial for resisting reactive oxygen species (ROS) [89]. Inhibition of the PPP reduces the level of NADPH, making bacteria more susceptible to ROS damage and disrupting the respiratory chain and altering membrane permeability. In our study, we also observed disruption of the redox state, significant increase in intracellular ROS and MDA, and significant decrease in ATP. This demonstrates the biological mechanism by which PCA regulates EMP and PPP, thereby interfering with energy metabolism. The oxidative stress state of the bacteria is not directly related to PCA itself, which is consistent with previous research on the use of PCA as an antioxidant and anti-inflammatory drug in the body [71]. This regulatory mechanism of metabolism can help us discover and screen effective antibacterial candidates.

After learning about the metabolic disorder caused by PCA, we reviewed the synergistic antibacterial mechanism of PCA again. The inhibition of biofilm formation and the change of membrane permeability may be due to this metabolic change, such as the regulation of the formation and dissociation of biofilm by succinic acid and dicarboxylic acid, which is an intermediate product of the citric acid cycle. At the same time, metabolism is also affected by the pentose phosphate pathway. Therefore, whether it is the destruction of EMP by PCA or the blockage of PPP, it will affect the formation of biofilm [90]. Cell membrane permeability is also the same. When the bacterial respiratory chain is damaged by reactive oxygen species, it will

cause the oxidation and lipid peroxidation of the cell membrane, thereby reducing the integrity and fluidity of the cell membrane and increasing the permeability of the cell membrane [91]. Therefore, the effect of PCA on metabolism will ultimately be more conducive to the entry of antibiotics into bacteria and play a role, especially the target of carbapenem antibiotics against CR-hvKP itself is on the inner membrane. With the successive collapse of the "natural resistance line" biofilm and cell membrane, the actual efficacy of antibiotics will be greatly improved.

Although we have demonstrated that PCA alters the endogenous oxidative stress of bacteria through metabolic pathways, PCA itself possesses strong reducing properties. Whether this reducing effect will weaken the oxidative stress caused by metabolic changes still needs further investigation. Meanwhile, our study found that under sub-inhibitory concentrations of PCA, the color of the bacterial liquid culture medium deepens with increasing drug concentration. The relationship between this change and metabolism is not clear and requires further exploration.

In conclusion, this study demonstrates that natural plant monomer protocatechuic acid has good antibacterial activity against CR-hvKP and can be used as an antibiotic adjuvant or biofilm inhibitor at low concentrations. It is a promising candidate drug for the development of new antibiotic drugs to combat drug-resistant bacterial pathogens related infections.

940

Abbreviations:

ATP, Adenosine Triphosphate; BPGM,2,3-Bisphosphoglycerate mutase; c-di-GMP, Cyclic di-GMP; CR-hvKP, Carbapenem-resistant hypervirulent Klebsiella pneumoniae; CRKP, Carbapenem-Resistant Klebsiella pneumoniae; DAPI, 4',6-diamidino-2-phenylindole; DHFR, Dihydrofolate reductase; DisC3(5), 3,3'-diheptylperoxy carbene-5,5'-dichlorofluorescein; DNA, Deoxyribonucleic Acid; ED, Phosphorylated sugar metabolism pathway; EMP, Glycolytic Pathway; FASR, Fatty Acid Synthesis Reaction; FICI, Fractional Inhibitory Concentration Index; G6PDH, Glucose-6-phosphate dehydrogenase; GAP, Glyceraldehyde-3-phosphate; GC-MS, Gas Chromatography-Mass Spectrometry; HEPES, 4-(2-hydroxyethyl)-1-piperazineethanesulfonic acid; HMGR, Hydroxymethylglutaryl-CoA Reductase; hvKP, Highly Virulent Pneumonia Klebsiella pneumoniae; KCL, Potassium Chloride; LB, Luria-Bertani medium; LC-MS, Liquid Chromatography-Mass Spectrometry; MBC, Minimum Bactericidal Concentration; MDA, Formaldehyde; MIC, Minimum Inhibitory Concentration; NADP(H), Nicotinamide Adenine Dinucleotide Phosphate (reduced form); NOS, Nitric Oxide Synthase; NR, Nitrate Reductase; NPN, Non-Protein Nitrogen; PCA, Pyrrolidone carboxylic acid; PDAM, 4-phenyl-2,4-diamino-5-methylpyridine; PI, Propyl iodide; PBS, Phosphate Buffered Saline; PPP, Pentose Phosphate Pathway; PYO, Pyrroloquinoline quinone; qRT-PCR, Quantitative Reverse Transcription Polymerase Chain Reaction; R5P, Ribose-5-phosphate; RNA, Ribonucleic Acid; ROS, Reactive Oxygen Species

942

Acknowledgements

This study has been made possible thanks to the support from National Key Research and Development Program of China (2023YFD1800100); as well as the joint funding from the National Natural Science Foundation of China (U22A20523).

943

References

[1] Podschun R, Ullmann U. Klebsiella spp. as nosocomial pathogens: epidemiology, taxonomy, typing methods, and pathogenicity factors. Clin Microbiol Rev. 1998, 11(4), 589-6031.

[2] Huang YH, Chou SH, Liang sw, et al. Emergence of anXDRand carbapenemase producing hypervirulent Klebsiellapneumoniae strain in Taiwan[J]. J Antimicrob Chemother, 2018, 73(8), 2039-2046.

[3] Zhang Y, Zeng J, Liu W, et al. Emergence of a hypervirulent carbapenem-resistant Klebsiella pneumoniae isolate from clinical infections in China. J Infect. 2015, 71(5), 553-602.

[4] Mathers AJ, Stoesser N, Sheppard AE, et al. Klebsiella pneumoniae carbapenemase (KPC)-producing K. pneumoniae at a single institution: insights into endemicity from whole-genome sequencing. Antimicrob Agents Chemother. 2015, 59(3), 1656-63.

[5] Cowan MM. Plant products as antimicrobial agents. Clin Microbiol Rev. 1999, 12(4), 564-824.

[6] Cushnie TP, Lamb AJ. Antimicrobial activity of flavonoids. Int J Antimicrob Agents. 2005, 26(5), 343-565.

[7] Mahomoodally MF, Gurib-Fakim A, Subratty AH. Antimicrobial activities and phytochemical profiles of endemic medicinal plants of Mauritius. Pharm Biol. 2005, 43(3),

237-426.

[8] Zhang L, Ravipati AS, Koyyalamudi SR, et al. Antioxidant and anti-inflammatory activities of selected medicinal plants containing phenolic and flavonoid compounds. J Agric Food Chem. 2011, 59(23), 12361-77.

[9] Lee YS, Kang YH, Jung JY, et al. Protein glycation inhibitors from the fruiting body of Phellinus linteus. Biol Pharm Bull. 2008, 31(10), 1968-728.

[10] AbouAitah K, Piotrowska U, Wojnarowicz J, Swiderska-Sroda A, El-Desoky AHH, Lojkowski W. Enhanced Activity and Sustained Release of Protocatechuic Acid, a Natural Antibacterial Agent, from Hybrid Nanoformulations with Zinc Oxide Nanoparticles. Int J Mol Sci. 2021, 22(10), 5287.

[11] Srivastava N, Tiwari S, Bhandari K, Biswal AK, Rawat AKS. Novel derivatives of plant monomeric phenolics: act as inhibitors of bacterial cell-to-cell communication. Microb Pathog. 2020, 141, 103856.

[12] Parvekar P, Palaskar J, Metgud S, Maria R, Dutta S. The minimum inhibitory concentration (MIC) and minimum bactericidal concentration (MBC) of silver nanoparticles against Staphylococcus aureus. Biomater Investig Dent. 2020, 7(1), 105-109.

[13] Foerster S, Unemo M, Hathaway LJ, Low N, Althaus CL. Time-kill curve analysis and pharmacodynamic modelling for in vitro evaluation of antimicrobials against Neisseria gonorrhoeae. BMC Microbiol. 2016, 16, 216.

[14] Hashemi SS, Saadatjo Z, Mahmoudi R, et al. Preparation and evaluation of polycaprolactone/chitosan/Jaft biocompatible nanofibers as a burn wound dressing. Burns. 2022, 48(7), 1690-1705.

[15] Oddo, A., & Hansen, P. R. Hemolytic activity of antimicrobial peptides. In Antimicrobial peptides. Humana Press, New York, NY, 2017. Pp, 427-435.

[16] Bai S, Wang J, Yang K, et al. A polymeric approach toward resistance-resistant antimicrobial agent with dual-selective mechanisms of action. Sci Adv. 2021, 7(5), eabc9917.

[17] Aubry R, Buyck J, Prouvensier L, Decousser J-W, Nordmann P, Wicha SG, et al. An improved PKPD modeling approach to characterize the pharmacodynamic interaction over time between ceftazidime/avibactam and colistin from in vitro time-kill experiments against multidrug-resistant Klebsiella pneumoniae isolates. Antimicrob Agents Chemother. 2023, 67(10), e0030123.

[18] Vuotto C, Longo F, Pascolini C, Donelli G, Balice MP, Libori MF, et al. Biofilm formation and antibiotic resistance in Klebsiella pneumoniae urinary strains. J Appl Microbiol. 2017, 123(4), 1003-1018.

[19] Ommen P, Zobek N, Meyer R L. Quantification of biofilm biomass by staining: Non-toxic safranin can replace the popular crystal violet [J]. Journal of microbiological methods, 2017, 141, 87-89.

[20] Rühmann B, Schmid J, Sieber V. Methods to identify the unexplored diversity of microbial exopolysaccharides. Front Microbiol. 2015, 6, 565.

[21] Takahashi C, Sato M, Sato C. Biofilm formation of Staphylococcus epidermidis imaged using atmospheric scanning electron microscopy. Anal Bioanal Chem. 2021, 413(30), 7549-7558.

[22] Halder, S., Yadav, K.K., Sarkar, R. et al. Alteration of Zeta potential and membrane permeability in bacteria: a study with cationic agents. SpringerPlus. 2015, 4, 672.

[23] Te Winkel JD, Gray DA, Seistrup KH, Hamoen LW, Strahl H. Analysis of Antimicrobial-Triggered Membrane Depolarization Using Voltage Sensitive Dyes. Front Cell Dev Biol. 2016, 4, 29.

[24] Rampersad SN. Multiple applications of Alamar Blue as an indicator of metabolic function and cellular health in cell viability bioassays. Sensors (Basel, Switzerland). 2012, 12(9), 12347-12360.

[25] Hartl J, Kiefer P, Kaczmarczyk A, Mittelviefhaus M, Meyer F, Vonderach T, et al. Untargeted metabolomics links glutathione to bacterial cell cycle progression. Nat Metab. 2020, 2(2), 153-166.

[26] Ran Y, Yang Q, Zeng J, Li F, Cao Y, Xu Q, et al. Potential xylose transporters regulated by CreA improved lipid yield and furfural tolerance in oleaginous yeast Saitozyma podzolica zwy-2-3. Bioresour Technol. 2023, 386, 129413.

[27] Wen G, An W, Chen J, Maguire EM, Chen Q, Yang F, et al. Genetic and Pharmacologic Inhibition of the Neutrophil Elastase Inhibits Experimental Atherosclerosis. J Am Heart Assoc. 2018, 7(4), e008187.

[28] Jumper J, Evans R, Pritzel A, Green T, Figurnov M, Ronneberger O, et al. Highly accurate protein structure prediction with AlphaFold. Nature. 2021, 596(7873), 583-589.

[29] Waterhouse A, Bertoni M, Bienert S, Studer G, Tauriello G, Gumienny R, et al. SWISS-MODEL: homology modelling of protein structures and complexes. Nucleic Acids Res. 2018, 46(W1), W296-W303

[30] Forli S, Huey R, Pique ME, Sanner MF, Goodsell DS, Olson AJ. Computational protein-ligand docking and virtual drug screening with the AutoDock suite. Nat Protoc.

2016 , 11(5), 905-19.

[31] Lai X, Zhong Z, Lin B, Wu Y, Ma Y, Zhang C, et al. RNA-seq and qRT-PCR analyses reveal the physiological response to acute hypoxia and reoxygenation in Epinephelus coioides. Front Physiol. 2022, 13, 1049776.

[32] Zhang Y, Du X, He Z, Gao S, Ye L, Ji J, et al. A Vanadium-Based Nanoplatform Synergizing Ferroptotic-like Therapy with Glucose Metabolism Intervention for Enhanced Cancer Cell Death and Antitumor Immunity. ACS Nano. 2023, 17(12), 11537-11556.

[33] Jiang M, Jike Y, Liu K, Gan F, Zhang K, Xie M, et al. Exosome-mediated miR-144-3p promotes ferroptosis to inhibit osteosarcoma proliferation, migration, and invasion through regulating ZEB1. Mol Cancer. 2023, 22(1), 113.

[34] Chen X, Wo F, Jin Y, Tan J, Lai Y, Wu J.Drug-Porous Silicon Dual Luminescent System for Monitoring and Inhibition of Wound Infection.ACS Nano. 2017, 11(8), 7938-7949.

[35] Hrast M, Rožman K, Ogris I, Škedelj V, Patin D, Sova M, et al. Evaluation of the published kinase inhibitor set to identify multiple inhibitors of bacterial ATP-dependent mur ligases. J Enzyme Inhib Med Chem. 2019, 34(1), 1010-1017.

[36] Shapiro S S, Wilk M B. An analysis of variance test for normality (complete samples) [J]. Biometrika, 1965, 52(3/4), 591-611.

[37] Li J, Ye BC. Metabolic engineering of Pseudomonas putida KT2440 for high-yield production of protocatechuic acid. Bioresour Technol. 2021, 319, 124239.

[38] Akbar MU, Haque A, Liaquat S, Schierack P, Ali A. Biofilm Formation by Staphylococcus epidermidis and Its Inhibition Using Carvacrol, 2-Aminobenzemidazole, and 3-Indole Acetonitrile. ACS Omega. 2022, 8(1), 682-687.

[39] Wang L, Yuan L, Li ZH, Zhang X, Leung KMY, Sheng GP. Extracellular polymeric substances (EPS) associated extracellular antibiotic resistance genes in activated sludge along the AAO process: Distribution and microbial secretors. Sci Total Environ. 2022, 816, 151575.

[40] Galeazzi L, Groppa G, Giunta S. Mueller-Hinton broth undergoes visible oxidative color changes in the presence of peroxidase and hydrogen peroxide. J Clin Microbiol. 1990, 28(9), 2145-7.

[41] Jin X, Zhang X, Ding X, Tian T, Tseng CK, Luo X, et al. Sensitive bacterial Vm sensors revealed the excitability of bacterial Vm and its role in antibiotic tolerance. Proc Natl Acad Sci U S A. 2023, 120(3), e2208348120.

[42] Guo R, Luo X, Liu J, Lu H. Mass spectrometry based targeted metabolomics precisely characterized new functional metabolites that regulate biofilm formation in Escherichia coli. Anal Chim Acta. 2021, 1145, 26-36.

[43] Zarkan A, Liu J, Matuszewska M, Gaimster H, Summers DK. Local and Universal Action: The Paradoxes of Indole Signalling in Bacteria. Trends Microbiol. 2020, 28(7), 566-577.

[44] Kaushik V, Tiwari M, Joshi R, Tiwari V. Therapeutic strategies against potential antibiofilm targets of multidrug-resistant Acinetobacter baumannii. J Cell Physiol. 2022, 237(4), 2045-2063.

[45] Zhang S, Wang Y, Lu J, Yu Z, Song H, Bond PL, et al. Chlorine disinfection facilitates natural transformation through ROS-mediated oxidative stress. ISME J. 2021, 15(10), 2969-2985.

[46] Atale N, Gupta S, Yadav UC, Rani V. Cell-death assessment by fluorescent and

nonfluorescent cytosolic and nuclear staining techniques. J Microsc. 2014, 255(1), 7-19.

[47] Bajpai VK, Park I, Khan I, Alshammari FH, Kumar P, Chen L, et al. (-)-Tetrahydroberberrubine·acetate accelerates antioxidant potential and inhibits food associated Bacillus cereus in rice. Food Chem. 2021, 339, 127902.

[48] Pletzer D, Mansour SC, Hancock REW. Synergy between conventional antibiotics and anti-biofilm peptides in a murine, sub-cutaneous abscess model caused by recalcitrant ESKAPE pathogens. PLoS Pathog. 2018, 14(6), e1007084.

[49] Song M, Liu Y, Li T, Liu X, Hao Z, Ding S, et al. Plant Natural Flavonoids Against Multidrug Resistant Pathogens. Adv Sci (Weinh). 2021, 8(15), e2100749.

[50] Juba ML, Porter DK, Williams EH, Rodriguez CA, Barksdale SM, Bishop BM. Helical cationic antimicrobial peptide length and its impact on membrane disruption. Biochim Biophys Acta. 2015, 1848(5), 1081-91.

[51] Lewis KN, Liao R, Guinn KM, Hickey MJ, Smith S, Behr MA, et al. Deletion of RD1 from Mycobacterium tuberculosis mimics bacille Calmette-Guérin attenuation. J Infect Dis. 2003, 187(1), 117-23.

[52] Keller, Markus A., Turchyn, Alexandra V., Ralser, Markus. Non-enzymatic glycolysis and pentose phosphate pathway-like reactions in a plausible Archean ocean. Molecular Systems Biology. 2014, 10 (4), 725.

[53] Alfarouk, Khalid O., Ahmed, Samrein B. M., Elliott, Robert L., Benoit, Amanda, Alqahtani, Saad S., Ibrahim, Muntaser E., et al. The Pentose Phosphate Pathway Dynamics in Cancer and Its Dependency on Intracellular pH. Metabolites. 2020, 10 (7), 285.

[54] Murai K, Sasaki D, Kobayashi S, Yamaguchi A, Uchikura H, Shirai T, et al. Optimal Ratio

of Carbon Flux between Glycolysis and the Pentose Phosphate Pathway for Amino Acid Accumulation in Corynebacterium glutamicum. ACS Synth Biol. 2020, 9(7), 1615-1622.

[55] Guédon, E., & Martin-Verstraete, I. Cysteine metabolism and its regulation in bacteria. In Amino acid biosynthesis: pathways, regulation and metabolic engineering. Springer, Berlin, Heidelberg, 2006. pp. 195-218.

[56] Stincone A, Prigione A, Cramer T, Wamelink MM, Campbell K, Cheung E, et al. The return of metabolism: biochemistry and physiology of the pentose phosphate pathway. Biol Rev Camb Philos Soc. 2015, 90(3), 927-63.

[57] Tang H, Ju X, Zhao J, Li L. Engineering ribose-5-phosphate isomerase B from a central carbon metabolic enzyme to a promising sugar biocatalyst. Appl Microbiol Biotechnol. 2021, 105(2), 509-523.

[58] Guo W, Gao J, Wang HJ, Su RY, Sun CY, Gao SH, et al. Phosphoglycerate Kinase Is Involved in Carbohydrate Utilization, Extracellular Polysaccharide Biosynthesis, and Cell Motility of Xanthomonas axonopodis pv. glycines Independent of Clp. Front Microbiol. 2020, 11, 91.

[59] Talwar D, Miller CG, Grossmann J, Szyrwiel L, Schwecke T, Demichev V, Mikecin Drazic AM, Mayakonda A, Lutsik P, Veith C, Milsom MD, Müller-Decker K, Mülleder M, Ralser M, Dick TP. The GAPDH redox switch safeguards reductive capacity and enables survival of stressed tumour cells. Nat Metab. 2023, 5(4), 660-676.

[60] Lee J, Lee J, Cho Y, Choi J, Han SW. A putative 2,3-bisphosphoglycerate-dependent phosphoglycerate mutase is involved in the virulence, carbohydrate metabolism, biofilm formation, twitching halo, and osmotic tolerance in Acidovorax citrulli. Front Plant Sci. 2022,

13, 1039420.

[61] Fraser HI, Kvaratskhelia M, White MF. The two analogous phosphoglycerate mutases of Escherichia coli. FEBS Lett. 1999, 455(3), 344-8.

[62] Zhu J, Schwörer S, Berisa M, Kyung YJ, Ryu KW, Yi J, et al. Mitochondrial NADP(H) generation is essential for proline biosynthesis. Science. 2021, 372(6545), 968-972.

[63] Laventie BJ, Jenal U. Surface Sensing and Adaptation in Bacteria. Annual Review of Microbiology. Annual Reviews. 2020, 74 (1), 735–760.

[64] POLLAK N, DÖLLE C, ZIEGLER M. The power to reduce: pyridine nucleotides – small molecules with a multitude of functions[J/OL]. Biochemical Journal, 2007, 205-218.

[65] Ezraty B, Gennaris A, Barras F, Collet JF. Oxidative stress, protein damage and repair in bacteria[J]. Nature Reviews Microbiology. 2017, 15(7), 385-396.

[66] Kwun MS, Lee DG. Ferroptosis-Like Death in Microorganisms: A Novel Programmed Cell Death Following Lipid Peroxidation. J Microbiol Biotechnol. 2023, 33(8), 992-997.

[67] Chinemerem Nwobodo, D., Ugwu, M. C., Oliseloke Anie, C., Al-Ouqaili, M. T., Chinedu Ikem, J., Victor Chigozie, U., & Saki, M. Antibiotic resistance: The challenges and some emerging strategies for tackling a global menace. Journal of clinical laboratory analysis, 2022, 36(9), e24655.

[68] Ciriminna R, Fidalgo A, Meneguzzo F, Presentato A, Scurria A, Nuzzo D, et al. Pectin: A Long-Neglected Broad-Spectrum Antibacterial. ChemMedChem. 2020, 15(23), 2228-2235.

[69] Félix G, Soto-Robles CA, Nava E, Lugo-Medina E. Principal Metabolites in Extracts of Different Plants Responsible for Antibacterial Effects. Chem Res Toxicol. 2021, 34(9), 1970-1983.

[70] Zhang, S., Z. Gai, T. Gui, J. Chen, Q. Chen and Y. Li. Antioxidant Effects of Protocatechuic Acid and Protocatechuic Aldehyde: Old Wine in a New Bottle. Evid. Based Complement. Alternat. Med. 2021, 6139308.

[71] Li Q, Liu X, Du Y, Zhang X, Xiang P, Chen G, et al. Protocatechuic acid boosts continual efferocytosis in macrophages by derepressing KLF4 to transcriptionally activate MerTK. Sci Signal. 2023, 16(786), eabn1372.

[72] Liu L, Zeng X, Zheng J, Zou Y, Qiu S, Dai Y. AHL-mediated quorum sensing to regulate bacterial substance and energy metabolism: A review. Microbiol Res. 2022, 262, 127102.

[73] Rice AM, Long Y, King SB. Nitroaromatic Antibiotics as Nitrogen Oxide Sources. Biomolecules. 2021, 11(2), 267.

[74] Zhao F, Wang XD, Erber LN, et al. Binding pocket alterations in dihydrofolate synthase confer resistance to para-aminosalicylic acid in clinical isolates of Mycobacterium tuberculosis. Antimicrob Agents Chemother. 2014, 58(3), 1479-87.

[75] Zhang S, Yang MJ, Peng B, Peng XX, Li H. Reduced ROS-mediated antibiotic resistance and its reverting by glucose in Vibrio alginolyticus. Environmental Microbiology. 2020, 22(10), 4367-4380.

[76] Perry EK, Meirelles LA, Newman DK. From the soil to the clinic: the impact of microbial secondary metabolites on antibiotic tolerance and resistance. Nat Rev Microbiol. 2022, 20(3), 129-142.

[77] Povolotsky TL, Keren-Paz A, Kolodkin-Gal I. Metabolic Microenvironments Drive Microbial Differentiation and Antibiotic Resistance. Trends Genet. 2021, 37(1), 4-8.

[78] Li Z, Gong T, Wu Q, Zhang Y, Zheng X, Li Y, Ren B, et al. Lysine lactylation regulates

metabolic pathways and biofilm formation in Streptococcus mutans. Sci Signal. 2023, 16(801), eadg1849.

[79] Wei Y, Tong Y, Zhang Y. New mechanisms for bacterial degradation of sulfoquinovose. Biosci Rep. 2022, 42(10), BSR20220314.

[80] Raven, P., G. Johnson, K. Mason and J. J. B.-N. Y. M.-H. Losos SR Singer How cells harvest energy. New York: McGraw-Hill, 2014.

[81] Reece, J. B., L. A. Urry, M. L. Cain, S. A. Wasserman, P. V. Minorsky and R. B. J. C. b. JacksonCellular respiration and fermentation. San Francisco, CA: Pearson, 2011.

[82] Alvarez-Santullano N, Villegas P, Mardones MS, Durán RE, Donoso R, González A, et al. Genome-Wide Metabolic Reconstruction of the Synthesis of Polyhydroxyalkanoates from Sugars and Fatty Acids by Burkholderia Sensu Lato Species. Microorganisms. 2021, 9(6), 1290.

[83] Cho ES, Cha YH, Kim HS, Kim NH, Yook JI. The Pentose Phosphate Pathway as a Potential Target for Cancer Therapy. Biomol Ther (Seoul). 2018, 26(1), 29-38.

[84] Wu YQ, Zhang CS, Xiong J, et al. Low glucose metabolite 3-phosphoglycerate switches PHGDH from serine synthesis to p53 activation to control cell fate. Cell Res. 2023, 33(11), 835-850.

[85] Keller MA, Zylstra A, Castro C, Turchyn AV, et al. Conditional iron and pH-dependent activity of a non-enzymatic glycolysis and pentose phosphate pathway. Sci Adv. 2016, 2(1), e1501235.

[86] Ge T, Yang J, Zhou S, Wang Y, Li Y, Tong X. The Role of the Pentose Phosphate Pathway in Diabetes and Cancer. Front Endocrinol (Lausanne). 2020, 11, 365.

[87] Foster JM, Davis PJ, Raverdy S, Sibley MH, Raleigh EA, Kumar S, Carlow CK. Evolution of bacterial phosphoglycerate mutases: non-homologous isofunctional enzymes undergoing gene losses, gains and lateral transfers. PLoS One. 2010, 5(10), e13576.

[88] Liu Q, Zhu F, Liu X, Lu Y, Yao K, Tian N, Tong L, et al. Non-oxidative pentose phosphate pathway controls regulatory T cell function by integrating metabolism and epigenetics. Nat Metab. 2022, 4(5), 559-574.

[89] Zhou G, Peng H, Wang YS, Li CL, Shen PF, Huang XM, et al. Biological functions of nirS in Pseudomonas aeruginosa ATCC 9027 under aerobic conditions. J Ind Microbiol Biotechnol. 2019, 46(12), 1757-1768.

[90] Kaila VRI, Wikström M. Architecture of bacterial respiratory chains. Nat Rev Microbiol. 2021, 19(5), 319-330.

944